

Measurements of Total Cross Sections for K_2^0 Mesons on Protons and Selected Nuclei from 168 to 343 MeV/c and Measurement of the K_2^0 Mean Life*†

G. A. SAYER‡ AND E. F. BEALL

Department of Physics and Astronomy, University of Maryland, College Park, Maryland 20740

AND

T. J. DEVLIN,§ P. SHEPARD, AND J. SOLOMON||

*Princeton-Pennsylvania Accelerator and Palmer Physical Laboratory,
Princeton University, Princeton, New Jersey 08540*

(Received 21 December 1967)

We have measured K_2^0 - p total cross sections for K_2^0 laboratory momenta between 168 and 343 MeV/c. From these data we have determined the isotopic spin-1 $\bar{K}N$ s -wave scattering length to be $(0.00 \pm 0.14) \pm i(0.62 \pm 0.06)$ F. This is in fair agreement with previous determinations. We have also measured K_2^0 -nuclear total cross sections for seven species of nuclei which span the periodic table, in the same momentum range, to statistical accuracies of typically a few percent in each of eleven momentum intervals within the range. The data at the highest momentum do not obey an $A^{2/3}$ law. We have also measured the K_2^0 mean life to be $(5.15 \pm 0.14) \times 10^{-8}$ sec. This is in agreement with previous results and represents an improvement in statistical accuracy by about a factor of 3. We have also studied K_2^0 and γ production at 93° by 2.8-GeV protons on 1.5-in. platinum. The experiment was performed using a scintillation-counter K_2^0 detector. Kinematic identification of each K_2^0 particle was made using a time-of-flight method: The bunched time structure of the internal proton beam of the Princeton-Pennsylvania accelerator was used to determine K_2^0 production times, and an electronic chopping technique was used to eliminate unwanted proton bunches. Depending upon beam conditions, between 10^3 and 10^4 useful K_2^0 mesons per hour were detected with momentum resolution of a few percent. In conjunction with the timing calibration of the system, we have made a direct velocity measurement of the relativistic limiting speed for electrons. The result is $(1 - \beta_{\max}) = 0.005 \pm 0.005$.

I. INTRODUCTION

WE have measured total cross sections for K_2^0 mesons on hydrogen,[¶]beryllium, carbon, aluminum, iron, copper, lead, and uranium for kaon laboratory momenta between 168 and 343 MeV/c, and we have measured the K_2^0 mean life. The experiment was performed at the Princeton-Pennsylvania accelerator (PPA). We used a technique which is well known in nuclear physics but was new to high-energy physics, namely, the determination of neutral particle velocities by measurement of flight times from the internal target of a high-intensity accelerator. This technique had been suggested as being possible in principle,¹⁻³ due to the fact that secondary particles at the PPA are produced in groups with time widths short enough to allow comparison of the detection time of a given neutral particle with its production time. However, the group spacing is

normally ~ 33 nsec, so that flight times are only measured modulo (~ 33 nsec) with this method, and it had been thought that the resulting ambiguities would make practical application of the idea difficult. We were able to solve this ambiguity problem by using an electronic chopping system to eliminate alternate groups of protons in the internal beam. In this way an ~ 67 -nsec structure was achieved without any increase in the group time width. The remaining ambiguities were quite tolerable for our purposes.

Our measurements were made with a scintillation-counter device which monitored the K_2^0 momentum spectrum in a secondary beam during various changes in the beam. The total cross sections were determined from the changes in the momentum spectrum caused by inserting absorbers into the beam. The mean life was measured by monitoring the changes in the spectrum caused by decay in flight between different positions of the detection device along the beam.

It is possible to extract low-momentum \bar{K}^0 - p total cross sections from our K_2^0 - p total cross sections and to thereby study the Dalitz-Tuan parametrization of the $\bar{K}N$ system at low energies.⁴ Our method is sensitive to combinations of the Dalitz-Tuan parameters different from those involved in the classic measurements of K^- - p partial cross sections.⁵⁻⁸ These latter measurements

* Work performed under the auspices of the U. S. Atomic Energy Commission.

† Portions of this work submitted by G. A. Sayer to the faculty of the graduate school of the University of Maryland in partial fulfillment of the requirements for the degree of Doctor of Philosophy. G. A. Sayer, University of Maryland Technical Report No. 748 (unpublished).

‡ Present address: Haverford College, Haverford, Pa.

§ Present address: Rutgers—The State University, New Brunswick, N. J.

|| Present address: University of Illinois at Chicago Circle, Chicago, Ill.

¹ P. A. Piroué and A. J. S. Smith, IEEE Trans. Nucl. Sci. NS-12, 249 (1965).

² V. Fitch, C. Quarles, and H. Wilkins, Princeton-Pennsylvania Accelerator Technical Note No. A-101, 1964 (unpublished).

³ E. F. Beall, University of Maryland Technical Report No. 387, 1964 (unpublished).

⁴ R. H. Dalitz and S. F. Tuan, Ann. Phys. (N. Y.) 9, 391 (1960).

⁵ W. E. Humphrey and R. R. Ross, Phys. Rev. 127, 1305 (1963).

⁶ M. Sakitt, T. B. Day, R. G. Glasser, and N. Seeman, Phys. Rev. 139, B719 (1965).

⁷ J. K. Kim, Phys. Rev. Letters 14, 29 (1965).

⁸ G. S. Abrams and B. Sechi-Zorn, Phys. Rev. 139, B454 (1965).

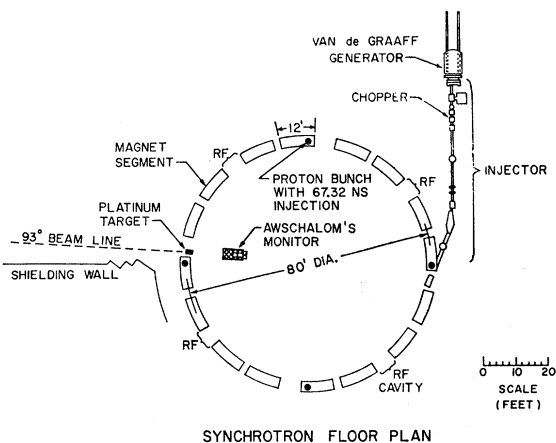


FIG. 1. Floor plan of the Princeton-Pennsylvania accelerator. The proton bunches and the platinum target are distorted for clarity.

were done with bubble chambers and thus are subject to experimental problems quite different from ours. We find essential agreement with the most recent of the bubble-chamber results.

Preliminary results of the experiment⁹ and our final result for the K_2^0 mean life¹⁰ have been given. The present paper is a complete report of the experiment.

II. EXPERIMENTAL DETAILS

In the following, Sec. II A deals with certain critical aspects of the synchrotron and its operation; Sec. II B with the secondary K_2^0 beam; Sec. II C with the K_2^0 detection system; Sec. II D with the timing system used to measure K velocities; and Sec. II E with miscellaneous details of the running of the experiment.

A. Synchrotron

A diagram of the PPA is shown in Fig. 1. The repetition rate is one magnet cycle per 53 msec. The maximum proton kinetic energy is 3.0 GeV. There are four rf acceleration cavities operating at a frequency which is about 30 Mc/sec near the end of each cycle. This frequency is the 8th harmonic of the proton orbit frequency and thus eight phase-stable regions, known colloquially as "bunches" or "buckets," circulate around the circumference. The region of rf phase within which the acceleration is stable is $\sim 20^\circ$ near maximum energy, comparable to, but somewhat smaller than that of, other synchrotrons. Since the rf frequency is large, the bunches are short; they are ~ 2 ft in length or ~ 2 nsec in time width near maximum energy.

The time width of the protons striking the target is actually less than that of the bunches in stable orbit for the particular targeting technique used during our

experiment. The rf is frequency-modulated at spill time to shrink the orbit so that the beam grazes a beryllium lip on the outer side of the target. The energy loss in the lip is such that the beam strikes the center of the target after one additional turn, during which time the change in the proton-rf relative phase is negligible. While each proton bunch moves slowly inward, taking ~ 5 msec to completely pass the target lip, synchrotron oscillation causes the bunch to rotate about its center at a rapid rate, ~ 17 kc/sec. Thus the targeting process is similar to the peeling of an onion. The time width of the protons striking the target for each "cut" is just the length of the cut itself, not that of the bunch. Kitagaki has made estimates of the on-target time width, assuming the above mechanism and taking into account other effects such as betatron oscillations.¹¹ He estimates the time width to be roughly constant at ~ 0.7 nsec over the spill.

The on-target time width is comparable to the resolving times obtainable with present-day counting equipment and is therefore difficult to measure by observation of the time structure of secondary particles. Various studies have been made¹² and the apparent widths, including coincidence resolution and other effects, have been in the range of a few nsec, depending upon the circuits, counters, and timing methods used. Our measurements with a γ -ray detector which is described in Sec. II B gave a time width of 2.0-nsec full width at half-maximum (FWHM) including various circuit effects. Strovink has made measurements wherein he determines his resolution effects, essentially by adding extra counters to coincidence requirements and by observing the resulting increases in apparent width.¹³ He quotes a figure of 1.06 nsec for the on-target time width, somewhat larger than the above estimate.

Knowledge of the exact time structure of the beam on target is not necessary in order to make time-of-flight measurements as long as the structure is stable. However, the targeting process in general causes changes in the equilibrium value of the rf-proton relative phase during the spill and, further, long-term drifts in the phase can occur as a result of normal fine tuning of the machine. We made a controlled study of the dependence of the phase upon the cavity modulation by varying tuning parameters while timing secondary γ rays with respect to the rf. We observed phase variations over the spill of order 1 nsec and changes in the average (i.e., averaged over the spill) phase due to tuning adjustments which were typically $\frac{1}{2}$ nsec but were considerably larger for extreme changes in the modulation. During actual data taking in the experiment, the timing effects caused by rf-proton relative phase changes during the spill

¹¹ T. Kitagaki, Princeton-Pennsylvania Accelerator Technical Note No. A-215, 1965 (unpublished).

¹² References 1, 2, and 21; D. Hutchinson (private communication).

¹³ M. W. Strovink, Princeton-Pennsylvania Accelerator Technical Note No. A-243, 1966 (unpublished).

⁹ E. F. Beall, G. Sayer, T. J. Devlin, P. Shepard, and J. Solomon, Bull. Am. Phys. Soc. **11**, 326 (1966).

¹⁰ T. J. Devlin, J. Solomon, P. Shepard, E. F. Beall, and G. A. Sayer, Phys. Rev. Letters **18**, 54 (1967).

were minimized in a manner to be discussed in Sec. II D, and the residual effects just contributed a small amount to our total time resolution. Long-term drifts in the *average* phase caused by tuning could have produced tuning-dependent drifts in the flight-time measurements. Therefore an effort was made during data taking to perform the necessary tuning of the spill in such a way as to minimize the phase drifts. The drifts were then typically 0.2 nsec between calibrations. Furthermore, their effects were eliminated by adjusting cable delay (see Sec. II D).

The target spill for our experiment occurred over a 5-msec period ending at maximum energy. During this interval the rf changed from 29.6 to 29.8 Mc/sec and the proton energy from 2.4 to 3.0 GeV. The 5-msec spill was actually uniform for a period of typically 3–4 msec—except for synchrotron structure and the basic rf structure. The value of the rf with chopper off (see below), averaged over the spill and weighted by the actual distribution of secondary particles, was 33.66 nsec. Fluctuations in this average were $\sim 0.1\%$. The proton energy, averaged in the same way, was 2.8 GeV with fluctuations of less than 0.1 GeV.

The stability of the targeting mechanism was such that, after leaving the lip, the average transverse (i.e., radial) position of the protons in striking the target was constant within $\sim 20 \mu$ (as determined by comparison of the rates in different monitor telescopes, see Sec. II B). Fluctuations in the amount of beam actually striking the lip were $\sim 20\%$ (as determined by comparison of an induction electrode signal with the rate in a monitor telescope).

The timing ambiguities associated with measuring flight times modulo (~ 33 nsec) would have been quite severe for our purposes, and it was therefore desirable to modify the beam structure in the synchrotron so as to increase the natural bunch spacing. This was achieved by eliminating alternate bunches at injection time. A chopping system was instrumented as follows.

A signal was obtained from the rf master oscillator and counted down with a scale-of-two. The scaler output was shaped, amplified to ~ 2 kV, and transmitted to a pair of deflection plates situated in the 3-MeV injector at a point 60 ft from the entrance to the synchrotron ring (cf. Fig. 1). The plates were 10 in. in length along the injector beam line, 4.5 in. in width, and were separated by 1.5 in. The width and phase of the chopper signal were adjusted so as to cover alternate phase-stable regions in the ring. The vertical deflection of ~ 1.5 in. at the entrance to the ring was sufficient to drive protons out of these regions. Thus alternate bunches only were accelerated. The bunch spacing was 67.32 nsec at average spill time.

The chopping system was not perfectly efficient. It was usually necessary to adjust steering electrodes in the injector in order to maintain the fraction of accelerated beam in the “wrong” alternate bunches at a very low level. We obtained instantaneous estimates of this

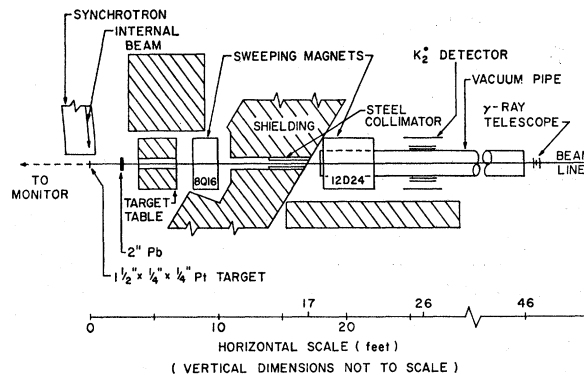


Fig. 2. Layout diagram showing the K_2^0 beam components. Six of the twelve counters comprising the detector are indicated.

fraction by observation of induction electrode signals, and we measured its average over extended periods of time accurately with our γ -ray telescope. The fraction was less than 1% at all times during data taking. The inefficiency was believed to have resulted from the fact that the synchrotron's master timing circuitry, hence the chopper, is activated for a given machine cycle only after some beam is injected into the ring.

A low-level signal was extracted from the countdown circuit in parallel with the chopper signal for use as an approximate time reference for the bunches actually containing beam. It was used to gate a signal from the master oscillator, the latter signal being the actual time reference for our time-of-flight measurements (see Sec. II D). Injection ended after ~ 8 orbits in a given machine cycle, but the low-level chopper signal was maintained until the end of the cycle in order to provide an alternate-bunch time reference at spill time. Since it was driven ultimately by the master oscillator, it tracked the signal used for the actual time reference throughout the rf variations. The number of counts skipped by the countdown circuit after injection was less than one count per thousand machine cycles.

The injection at the PPA is dc in normal (i.e., unchopped) operation, but presumably the injected protons which do not enter phase-stable regions are not accelerated. Therefore, activation of the chopping system should reduce the beam intensity by exactly 2. Under optimum controlled conditions this was indeed found to be true, within measurement accuracy. However, among other things, the tuning of the machine is easier to maintain at higher intensities and the beam intensity, averaged over long times, for chopped operation was usually somewhat less than $\frac{1}{2}$ that for normal operation.

It was also possible to operate the synchrotron with ~ 134 -nsec structure by adding another scale-of-two to the countdown circuit, adjusting the output pulse to exclude three out of every four proton bunches. The three “wrong” bunches during ~ 134 -nsec operation contained differing amounts of beam; however, each contained only of the order of 10^{-3} of the beam in the

one "right" bunch, the same contamination as for ~ 67 -nsec operation under typical conditions.

B. K_2^0 Beam

A layout of the secondary beam is shown in Fig. 2. The beam was taken at an angle of 93° into what is known as the "meson area." The general design was that of a simple neutral beam with a solid angle of 75.5μ sr. From our measurements and those of others,¹⁴ $\sim 30 K_2^0$ mesons, $\sim 10^4$ neutrons, and $\sim 10^4$ γ rays per 10^{10} protons on target (a typical rate per machine cycle) emerged from the target into this beam. The γ rays were largely removed with a lead filter. Allowing for decay in flight, the neutron to K_2^0 ratio was of order 10^3 at a typical position of the K_2^0 detector.

The internal target was platinum, $1\frac{1}{2}$ in. along the internal beam, $\frac{1}{4}$ in. \times $\frac{1}{4}$ in. in cross section. Two sweeping magnets were used. The first was an 8Q16 quadrupole, wired as a dipole and shimmed to a 3-in. horizontal gap (thus sweeping vertically). It cleared charged particles originating in the production target and in the cross-section targets. Its operating current of 800 A yielded a measured field of 8 kG. The second magnet, a 12D24 dipole with 6-in. gap operating at 300 A, eliminated charged particles resulting from secondary interactions in the collimator walls.

The limiting beam aperture was a 2-in.-diam circle at a point 204 in. from the internal target. Thus at 26 ft from the target, for example, the horizontal beam distribution in the median plane, with the target described above, consisted of an umbra 2.3 in. in width and a penumbra of 0.8 in. on either side. The vertical distribution at the center line, again at 26 ft, had a total width of 3.1 in. with negligible penumbra. Beam profiles, taken with a small probe counter, verified both the centering and the distribution of the beam expected from the geometry.

A remote-controlled table with four vertical positions, 36 in. in length along the beam and 30-in. wide, was positioned with its center $5\frac{1}{2}$ ft from the internal target. It supported the targets used for the cross-section measurements and a layer of lead used for plugging the beam port. The target sequence was: plug at bottom, 4-in. \times 4-in. open space, and two 4-in. \times 4-in. targets (except for the beryllium and copper targets, cf. Table II) above. The remaining parts of the target table were stacked with lead to the height of the top edge of the uppermost target. The γ -ray filter was a 2-in. lead brick, also removable by remote control, and was placed $2\frac{1}{2}$ ft from the internal target.

The beam was evacuated to better than 10μ Hg from the entrance of the second magnet to a point 46 ft from the internal target. The vacuum region was 6 in. in

height and 12 in. in width inside the magnet and 12 in. in diam with a $\frac{1}{8}$ -in. aluminum wall downstream of the magnet. The purpose of the vacuum was to eliminate background caused by neutron interactions in air. We verified that the residual gas did not cause background by operating the K_2^0 detector (which is described in Sec. II C) with the vacuum spoiled. Indeed, there was no evidence that the vacuum was actually necessary.

The main shielding wall was of steel, 6 ft in length along the direction of the neutral beam. It was supplemented with small concrete blocks in the area of the first magnet. Brass inserts were placed in the first magnet and formed a vertical aperture of 3 in. A wall of concrete was built along the right side of the beam line downstream of the second magnet. Its purpose was to shield our apparatus from equipment in neighboring secondary beams. Zinc bricks (not shown in Fig. 2) were placed to the sides of the beam inside the vacuum region in the second magnet, forming a horizontal aperture of $4\frac{7}{8}$ in. They gave some additional shielding and also provided a baffle against slit scattering of neutrons from the collimator.

The principal beam monitor for the experiment was Awschalom's monitor¹⁵ (also variously known as the "beam-on-target monitor," and "BOT"), which is a permanent facility consisting of a 3-counter telescope inside the synchrotron ring. It is indicated in Fig. 1. Its counting rate is about 3–4 per 10^{10} protons onto a $1\frac{1}{2}$ -in. Pt target.¹⁶ The Awschalom monitor was used to normalize all K_2^0 counting rates in our data analysis. Our secondary monitor was a γ -ray telescope at the end of the neutral beam (cf. Fig. 2). It consisted of an anti-counter, lead converter, counter, slow-proton absorber, and counter in that order. Its limiting counter was 1 in. in diam. Its counting rates were ~ 7 and ~ 130 counts per 10^{10} protons with the Pb filter in and out of the beam, respectively. This telescope was used as a check on the Awschalom monitor and for various other purposes to be discussed later.

The stability of the ratio of the rates in the two monitor telescopes was excellent. With only the Pb filter in the beam line there were measurable long-term drifts in this ratio, but they were less than 0.2% per day. These drifts may have been due to the fact that an appreciable fraction, $\sim 60\%$, of the counting rate in the γ -ray telescope with filter in was not due to γ rays (this was determined by timing the telescope with respect to the rf, see Sec. II D), and this component may have been rate-dependent to some extent. With the filter and all targets *out* of the neutral beam, there was no

¹⁵ M. Awschalom (unpublished).

¹⁶ All of our quoted flux measurements assume a figure of 3.5 counts in the Awschalom monitor per 10^{10} protons. In principle such flux measurements could be compared with others made at different angles and different times if all such measurements were normalized to this same monitor. However, one must be cautious in this regard because the detailed hardware around the target which is shown in Figs. 1 and 2 is periodically changed, sometimes altering the amount of material between the target and the monitor.

¹⁴ P. A. Piroué and A. J. S. Smith, Phys. Rev. 148, 1315 (1966). The neutron spectrum has not actually been measured. We have assumed for order-of-magnitude purposes that the neutron spectrum is the same as the measured proton spectrum.

evidence of any drift throughout our data-taking period: A statistical analysis was performed upon 17 short runs with filter and targets out, each with a statistical error of 1.6% in the monitor ratio, distributed over the experiment. The χ^2 was 15.4 for 16 degrees of freedom for the hypothesis that the ratios were statistically distributed about a single value.

The stability of the monitor ratio not only gives evidence for the reliability of the monitors; it also is sensitive to variations in the transverse (radial) distribution of the protons striking the internal target. This is because the γ rays traversed about a radiation length in leaving the target, while the (presumably strongly interacting) particles which counted in the Awschalom monitor traversed a very small fraction of an interaction length.¹⁷ We estimate that a drift in the monitor ratio of 0.7% during the entire experiment (roughly the maximum compatible with the results of the above statistical analysis) would have been consistent with a corresponding drift in the average proton radial position at the target of no more than 20 μ . The resulting effect upon the K_2^0 flux in our neutral beam would have been $\sim 0.02\%$.

From our data we incidentally measured the γ -ray flux in the 93° beam, up to a conversion-efficiency factor. We used the γ -ray telescope rate with filter and all targets out and applied a 5% correction for the fraction of the rate not due to γ rays. Our result for the γ flux (R_γ) at 93°, for protons of average energy 2.8 GeV incident upon 1.5 in. of platinum, times the probability P of conversion in $\frac{1}{4}$ -in. Pb with at least one electron having a residual range of 1.7 g/cm² C, is

$$R_\gamma P = (5 \pm 1) \times 10^{-3} \text{ per proton per sr.} \quad (1)$$

The error is primarily due to the uncertainty in calibrating the amount of beam striking the target. One would have to know the energy spectrum to be able to calculate P ; however, a reasonable estimate of P is 0.7.

C. K_2^0 Detection System

The basic idea of the detection scheme was: No charged particles except K_2^0 decay products emerge from a collimated, evacuated neutral beam. The detector itself was a scintillation-counter array which responded to two charged particles emerging at wide angles from the K_{e3} , $K_{\mu 3}$, or $\pi^+\pi^-\pi^0$ mode of K_2^0 decay.

An end-view schematic of the detector is shown in Fig. 3. Four scintillation-counter telescopes were placed symmetrically around the beam vacuum pipe. Proceeding outward from the beam, each telescope consisted of a 12-in. \times 24-in. \times $\frac{1}{2}$ -in. counter, a $\frac{1}{4}$ -in. slow-pion ab-

¹⁷ A drift in the radial targeting position would actually cause the counting rates in both monitors to change in the same direction. This is because, for sufficiently high photon energies, more photons are produced than absorbed in traversing a thin slab of material after already penetrating of the order of one radiation length. However, the drift in the charged particle detector would still be negligible in comparison with that in the γ detector.

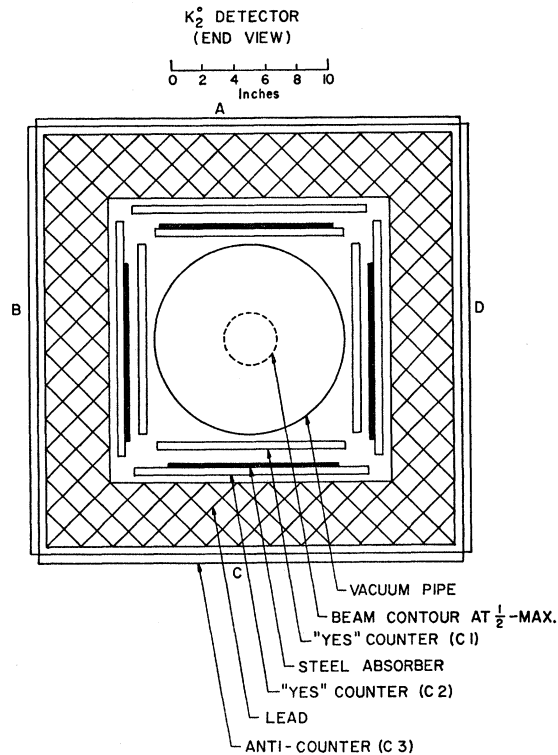


FIG. 3. End view of the K_2^0 detector. The half-maximum beam intensity contour is that at 26 ft from the internal target.

sorber, a 15-in. \times 24-in. \times $\frac{1}{2}$ -in. counter, a 4-in. layer of lead, and a 27-in. \times 36-in. \times $\frac{1}{2}$ -in. veto counter. The scintillation plastic was Nuclear Enterprises NE102. In plan view (not shown in the figure) the inner counters were centered along the beam line with respect to the veto counters, the iron extended for the lengths of the inner counters, and the lead extended for the lengths of the veto counters. The inner two counters of a given telescope counted a K_2^0 decay product and the veto counters rejected events caused by stray particles, mostly cosmic rays, originating outside the neutral beam. The 4 in. of lead was adequate to stop pions and muons from decays of kaons with the particular momentum distribution characteristic of the 93° beam, and to absorb all but a few percent of the electron showers. Thus the lead prevented the veto of legitimate events by the outer counters.

The design feature of placing the counters well out of the beam was optimum for the decays of K 's in our momentum region and also had the advantage that the rates for single counters were low, to the point where no rate-dependent effects were observed during the experiment. The energy available to the K_2^0 decay particles was somewhat more than $\frac{1}{2}$ the K rest energy while the energy available to protons knocked out of the vacuum pipe or inner counters by neutrons with energies typical of the 93° beam was generally less; and the small amount of iron between the first and second counters of

TABLE I. K_2^0 detector properties and counting rates.

Momentum (MeV/c) ^a	Detection efficiency (%)	Momentum resolution (% FWHM)	Counting rate ^b	Background rate ^b	$d^2N/d\Omega dp$ at target ^c [$10^{-4}/(\text{BeV}/c \text{ proton sr})$]
343	1.3	11	1665±14	186±19	1.15±0.03
308	1.5	10	1427±13	157±19	1.26±0.04
281	1.6	9	1212±12	107±16	1.37±0.05
258	1.8	8½	1055±11	70±10	1.39±0.04
239	1.9	8	921±10	60±12	1.59±0.06
223	2.1	7½	778± 9.6	45±12	1.53±0.06
209	2.2	7	655± 8.8	20± 6	1.49±0.05
197	2.4	7	546± 8.8	24± 6	1.51±0.07
187	2.5	6½	429± 7.1	21± 7	1.28±0.06
177	2.6	6½	339± 6.4	9± 2	1.23±0.07
168	2.7	6	271± 5.7	25± 7	1.03±0.08

^a The quoted momenta are averages over 7 channel flight-time bins.

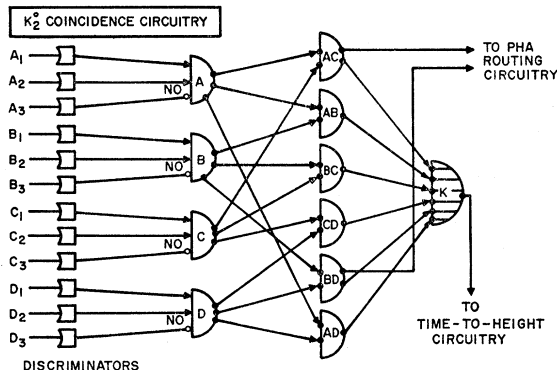
^b The quoted counting rates are sums over bins of width 7 channels = 13.6 nsec in flight time, with the detector 26 ft from the internal target, with only 2 in. Pb in the beam line, per 4×10^6 counts in the monitor. The errors are statistical only.

^c The quoted errors in the production spectrum include all known sources except for a 25% normalization uncertainty. They are dominated by the uncertainty in the correction for absorption by the γ filter.

each telescope attenuated the background by a great amount in comparison with the attenuation of K decay products.

The lightpipes of the counters were tapered in one dimension but not in the other and had constant ½-in. thickness; and this proved adequate for our purposes. They pointed downstream to partially compensate for geometric effects on the pulse timings (see Sec. III A). However, they were cut asymmetrically and fastened differently to the two inner counters of each telescope in such a way that the lightpipe overlap area was reduced. This precaution and the careful setting of the phototube voltages reduced lightpipe coincidences to less than 1% of the K counting rate. The photomultipliers were Amperex 56AVP. The base circuits were of a design, due to J. MacG. Dobbs and W. K. McFarlane, which is widely used at the PPA.

The detector was mounted on a cart which could roll on rails placed parallel to the beam line. This facilitated movement of the apparatus for the lifetime measurement. During such a translation the vacuum pipe was fixed and the counter array moved freely over it. The error in the centering of the apparatus at any detector position was less than ¼ in.

FIG. 4. K_2^0 coincidence system block diagram.

The following labeling conventions for the counters in the detector are used for the remainder of this paper: Starting from the top and proceeding clockwise while looking downstream along the beam, the telescopes are named A, B, C, and D, respectively. Proceeding from the inside of the detector to the outside, the A telescope counters are named A_1 , A_2 , and A_3 , respectively; and the same convention applies to the other telescopes.

A coincidence of any two counter telescopes was required as the signature of a K_2^0 event. A block diagram of the logic circuitry is shown in Fig. 4. The circuits were standard Chronetics modules except for the 6-fold OR. It consisted of a simple diode passive adder made with tunnel rectifiers, followed by a Chronetics module to shape the output signal. The discriminators immediately following the individual counters were adjusted for a 20-Mc/sec (nominal) maximum repetition rate in order to eliminate afterpulsing. The discriminators for the "1" and "2" counters in each telescope were output-clipped to provide dc restoration in the following circuits. The cabling was such that the transit times for each set of similar signals at each stage in the logic were identical to within ~ 0.2 nsec.

Some properties of the K_2^0 detector and some counting rates are given in Table I. Column 2 gives the calculated detection efficiency as a function of momentum. The calculations were performed using a Monte Carlo program which is discussed in Sec. III E. In addition, our result for the mean life, 51.5 nsec, and a branching ratio into charged decay modes of 0.78 were assumed.¹⁸ Specifically, each entry in the column is the probability that a K_2^0 with the appropriate momentum which reaches a point 36-in. upstream of the center of the detector will both decay and be detected (decays upstream of this point have a negligible probability of being detected). The efficiency decreases with momentum (due almost entirely to the $1/p$ decay proba-

¹⁸ T. J. Devlin and S. Barshay, Phys. Rev. Letters **19**, 881 (1967).

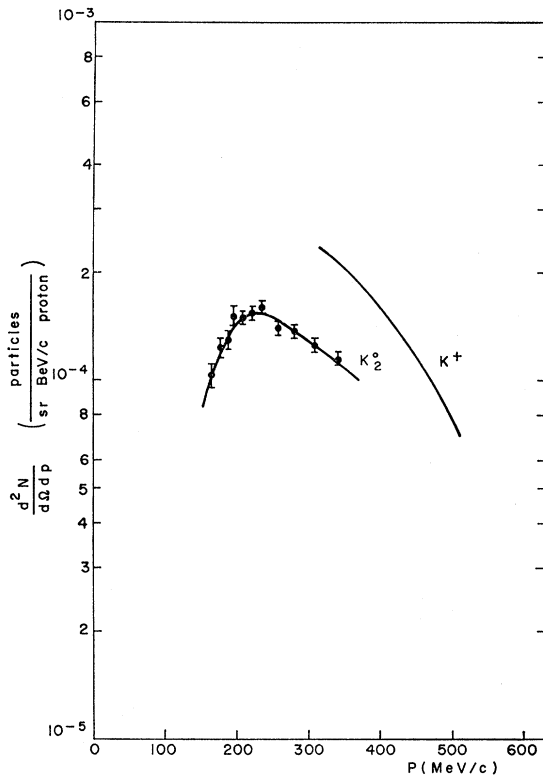


FIG. 5. The K_2^0 production spectrum at 93° for 2.8-GeV protons on 1.5 in. Pt obtained from this experiment, and the corresponding K^+ spectrum (Ref. 19). The smooth curve drawn through the K_2^0 spectrum has no fundamental significance.

bility factor) and is typically 2%. The FWHM momentum resolution, expressed in percent, is given in column 3. The quoted resolution is for the case of the center of the detector at 26 ft from the internal target. For other detector positions, it scales as the inverse of the target-to-detector distance. The resolution is in part empirical and in part calculated, as is discussed in Sec. III A. It is typically $\pm 4\%$ with the detector at 26 ft. The “raw” counting rates, with no cross-section targets in the beam and with the detector at 26 ft, are given in column 4, normalized to 4×10^5 counts in the Awschalom monitor. The corresponding background rates are given in column 5. The contributions to the background are: rates measured with the beam plugged (see Sec. II E), “ghosts” (Sec. II E), and beam-associated background (calculated from a fitting procedure which is described in Sec. III C).

We have used the information just discussed to calculate the K_2^0 production spectrum at the target for 2.8-GeV protons on $1\frac{1}{2}$ -in. Pt at a production angle of 93° . The background was subtracted; the rates were divided by the corresponding efficiencies; corrections for the attenuation by the Pb filter and by the air in the neutral beam ahead of the vacuum pipe were made, using our measured K_2^0 nuclear cross sections; and a correction was made for decay in flight from the internal

target, using 51.5 nsec (our result) for the mean life. The results are given in column 6 of Table I, and are also plotted in Fig. 5 together with the K^+ production spectrum. The latter was calculated using the results of Piroué and Smith.¹⁹ We have used a figure of 3.5 counts per 10^{10} protons in the Awschalom monitor¹⁶ in order to calculate the K_2^0 spectrum, and we estimate the absolute normalization uncertainty to be $\pm 25\%$. The corresponding uncertainty in the K^+ spectrum is $\pm 20\%$.¹⁹

The total raw counting rate for K momenta between 160 and 360 MeV/c, with the detector at 26 ft, was ~ 6000 /h at a typical internal beam intensity (1.0×10^{10} protons per pulse). The rates were reduced by factors of order 3 with a typical cross-section target in the beam, and by about 2 for a 15-ft displacement, the maximum displacement used for the lifetime measurement, of the detector away from the internal target. The drift in the total counting rate at fixed detector position with no targets in the beam was $\lesssim 1\%$ over a 12-h period. We measured accidental rates by delaying one telescope input to each of the two-telescope coincidence circuits (cf. Fig. 4) by 67 nsec. The accidentals were less than 0.2%. Event loss caused by random counts in the veto counters was measured to be less than 1%.

D. Timing System

We determined the times of flight of the detected K_2^0 mesons by measuring the difference in timing between the K signal and a signal from the rf master oscillator. The timing of the latter signal was related to the time at which a given group of protons struck the internal target, essentially by an additive constant. This constant was determined by measuring the time of flight of γ rays, whose velocity is of course known. A time-to-height conversion system and a pulse-height analyzer were used to store the flight-time information in digital form. Spectra detected by different combinations of

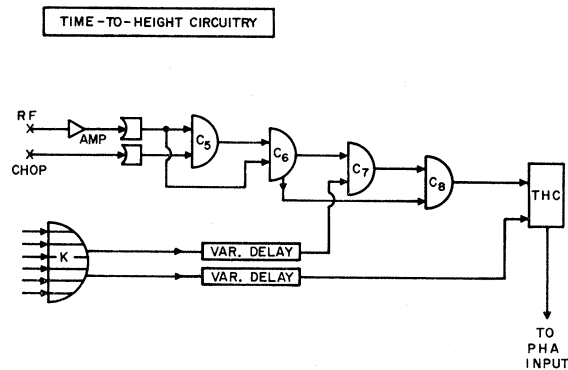


FIG. 6. Timing system block diagram.

¹⁹ Reference 14; we have corrected their results to correspond to a 1.5-in. target under the assumption that the attenuation of the proton beam in the target is 15% per inch. Their experiment was evidently run at a slightly different proton energy (2.9 GeV) than was ours, but we have made no corresponding correction.

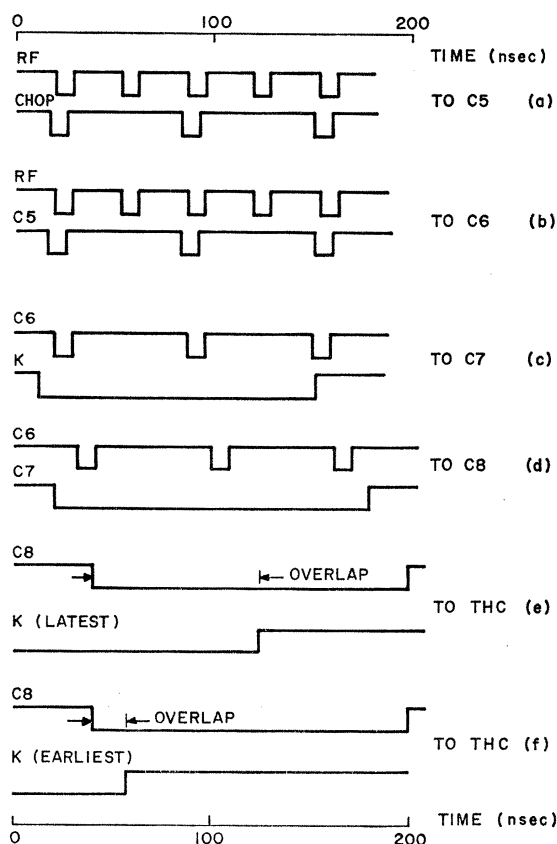


Fig. 7. Waveforms at the inputs to the timing circuits shown in Fig. 6. The pulses are all negative.

counter telescopes were stored in different memory banks of the analyzer. A detailed description follows.

The logic circuitry for the time-to-height conversion system is shown in Fig. 6. The electronics was Chronetics, the time-to-height converter (THC) itself a model 105 overlap circuit. The system had the following features: (a) stable, jitter-free time comparison with alternate rf cycles; (b) no start-stop ambiguity; (c) low rates at the THC inputs; and (d) no start pulse without a stop pulse and vice versa.

To understand the above points, refer to Fig. 6 and to the relevant waveforms which are shown in Fig. 7. A ~ 67 -nsec-period signal (CHOP), which gave a stable time reference to the alternate proton bunches actually comprising the beam, was derived from the system which chopped the injected beam (cf. Sec. II A). It was shaped and put in coincidence at C5 with a similarly shaped signal (RF) which was derived from the master oscillator. The signal called RF was used as the actual time reference throughout the system, the CHOP signal serving solely as a gate. A coincidence was made again at C6 with the RF input delayed enough to ensure that RF always determined the C6 output timing, independent of possible RF-CHOP relative time jitter.

The alternate-cycle time reference (C6) was gated by the K signal at C7 in order to accomplish features (c)

and (d) above. The K signal had all possible timings with respect to the RF. Therefore the K pulse sometimes determined the C7 timing, destroying the time reference. The reference was restored by putting the C6 and C7 pulses in coincidence at C8 with sufficient delay in the C6 input so that it (C6) always determined the C8 output timing. Thus the leading edge of the C8 pulse gave a stable reference to the on-target timing of the alternate proton bunches which actually contained beam, and the pulse appeared only in the event of a count in the K detector. The C8 time-reference pulse and another pulse from the K circuitry were sent to the THC.

The maximum spread in timing of the C8 time reference with respect to the K pulse was just the alternate-bunch spacing, ~ 67 nsec, because shifting the K pulse at C7 by ~ 67 nsec would simply cause the next C6 pulse to provide the time reference [see Fig. 7(c)]. The delays in the THC inputs were adjusted to give timings falling between the extremes which are shown in Figs. 7(e) and 7(f). The pulse widths were adjusted so that the leading edge of C8 always started the time overlap and so that the trailing edge of the K input always stopped it. The K pulse was clipped to ensure the stability of its trailing edge.

The only inputs to the circuitry of Fig. 6 which operated at high rates were of constant frequency. Thus, any possible time-slewing effects caused by rate-induced baseline shifts in the ac-coupled circuitry were also constant. Therefore, if such effects were present, they were absorbed in calibration. Furthermore, there was no time slewing in the K circuitry of Fig. 4, at least none past the primary discriminators, because the outputs of all "1" and "2" discriminators were clipped and because all other rates were low. The sum of the rates in the single telescopes was measured to be ~ 35 times the K rate itself. Accounting for synchrotron-oscillation structure, the corresponding instantaneous rate is ~ 5 kc/sec. Also, the Dobbs-McFarlane tube bases that we used are known to display no visible sag at a 20-Mc/sec rate.

Presumably, the circuitry of Fig. 6 could have been simplified somewhat, eliminating C5 and C6. A three-fold coincidence could have been used to gate the time reference with both the K signal and the chopper signal simultaneously.

The THC output was transmitted to a Nuclear Data ND130 512-channel analyzer. Adjustments were made to give a scale of ~ 2 channels/nsec. This corresponded to ~ 7 channels per resolution width, as is discussed later. We used the memory-address-addition feature of the ND130 to store three different sets of data in three different 128-channel banks. When the vertical pair of counter telescopes (A and C in Fig. 3) produced the K count, a signal derived from the appropriate two-telescope coincidence circuit (AC in Fig. 4) was used to add 128 locations to the memory address prior to storage. In similar fashion, 256 locations were added when the horizontal pair (BD) counted. Therefore, the

AC coincidences were stored in the second 128-channel bank, and the BD coincidences in the third. Events which counted in any of the four adjacent-telescope pairs (AB, AD, BC, and CD) were all stored in the first bank. The zero of the analyzer scale was suppressed so that minimum time overlap in the THC [cf. Fig. 7(f)] approximately corresponded to the first channel. The maximum time overlap (the minimum plus ~ 67 nsec) corresponded to about 130 channels. Pulses corresponding to more than 128 channels went into overflow and such events were lost.

The monitors and the electronics ahead of the THC were gated off during event processing. The gate was off from the time the last pulse entered the THC until the analyzer finished storing. Dead-time corrections to the results quoted in Secs. II B and II C for the γ -ray and K_2^0 fluxes were negligible.

The detector position along the beam was changed during the lifetime measurement. Each time this was done, the delays in the K inputs to the THC and to the C7 coincidence circuit (see Fig. 6) were changed in order to compensate for the change in flight time. The delays were such that events with flight times corresponding to $\beta (=v/c)=1$ were maintained at the same position on the analyzer scale. The cables used to vary the delay were *RG8U*. One pair of cables was in the circuitry at all times so that the delays due to connectors alone were constant. The maximum difference in cable length for two different detector positions was 10 ft. Each cable delay was measured by driving a Chronetics module with the cable under test connected from the output to the input and by measuring the output frequency with a precision frequency meter. Comparison of the frequencies for any two cables then gave the difference in delay of the cables. In this way the differences in compensation delays for any two detector positions were determined to within 0.05 nsec.

We calibrated the time origin of the system by running the detector on fast electron pairs in the following manner: The lead filter in the beam was removed, a thin lead radiator was placed at the exit of the collimator, and the second magnet was turned off. The time spectrum for such a run showed a peak corresponding to $\beta=1$ electron pairs, produced by γ rays at the radiator, striking the detector. In addition to yielding the zero calibration, such peaks gave a measure of the K_2^0 flight-time resolution, hence the momentum resolution of the detector. The peaks were of order 3 nsec in width, and were slightly asymmetric. Further discussion of the zero calibration and the resolution will be given in Sec. III A.

We used three methods to calibrate the analyzer scale in time units: (1) Pulses from the γ -ray telescope which was described in Sec. II B replaced the K pulses at the inputs to the THC and to the C7 coincidence circuit, all other cabling remaining unchanged, and the injector chopper was turned off. Thus, γ -ray peaks (2.0 nsec FWHM) spaced by 33.66 nsec were observed on the

analyzer. This calibration was also done using the K detector. (2) The K detector was physically moved through known distances without changing the compensating cables, and corresponding timing runs with the lead radiator at the collimator exit were compared. (3) The spectra for timing runs taken with different compensating cables but at fixed detector position were compared. For each of the three calibration methods, peaks appeared at different positions on the analyzer scale with shifts caused by known delays. The first method was the most accurate but the others agreed well. After detailed analysis, the scale factor was determined to be 1.937 ± 0.006 channels/nsec. It was stable, to within the quoted uncertainty, throughout the data-taking period. The linearity of the timing system was checked by replacing the K pulses at the THC and at C7 with pulses derived from a 1-kc/sec oscillator. This should have produced a uniform time spectrum. The sensitivity was such that 1% deviations from linearity would have been observed. The spectrum was flat over the part of the analyzer used later in the data analysis. Some end effects were observed within 10 channels of either end of each 128-channel bank.

Finally, we minimized some effects caused by variations in the synchrotron rf and in the proton-rf relative phase. As a result of frequency variation during the target spill, the absolute rf phase at a fixed length of time before or after a secondary particle is produced changes with the time during the spill at which the particle is produced. Our timing system effectively examined the rf phase at some such time before or after a K event. This time interval was due to various cable delays and other constants. If the time delay were large so that we compared the K pulse with an rf cycle appreciably different from the one associated with the production of the K in the internal target, then the time calibration would have been in error at one part of the spill relative to another part. The size of such an error can be calculated and is of the order of a few nsec across a 5-msec spill for a time delay of 500 nsec.²⁰ The error can be eliminated in principle by timing with respect to the "right" rf cycle. Proton-rf relative phase variations during the spill cause a similar effect; and one can also compensate for them to the extent that they are linear.²⁰ To eliminate these effects, we adjusted the gross cable delay in the rf signal between the master oscillator and our timing circuitry empirically until the shift in timing of the γ -ray telescope across the spill was minimized. The residual timing variation during the spill was about 1 nsec and was presumably caused by second-order proton-rf phase variations. This residual effect contributed a small amount to the width of our resolution function.

An error similar to the one discussed above could have arisen between the RF and CHOP signals (cf. Fig. 6). This would be the case if the delay in the RF signal

²⁰ T. J. Devlin, Princeton-Pennsylvania Accelerator Technical Note No. A-242, 1966 (unpublished).

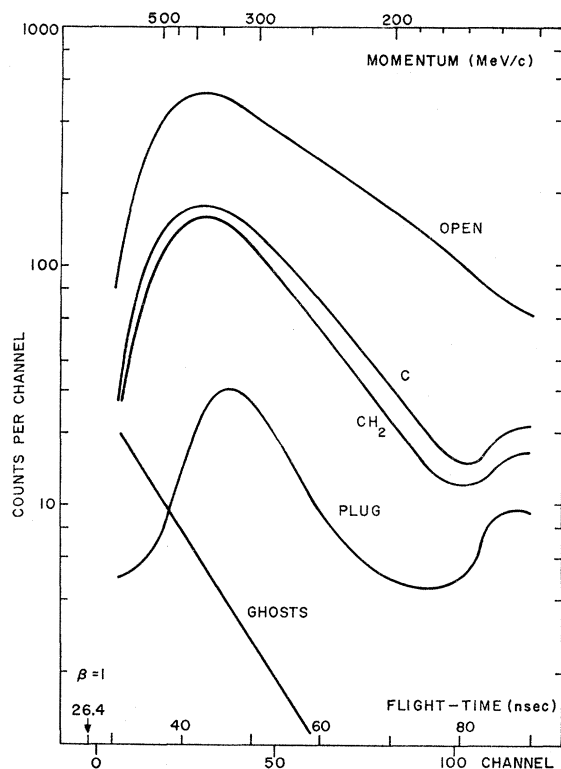


FIG. 8. Measured flight-time spectra with the detector at the 26-ft position, with no targets (open), carbon target (C), polyethylene target (CH_2), and beam plugged with 3 ft of lead (plug). The curve labelled "ghosts" is described in the text. All curves have the same normalization.

between the master oscillator and our timing circuitry were appreciably different than that in the CHOP signal from the master oscillator, through the injector chopper circuitry, to the timing circuitry. However, we verified, as discussed earlier, that the RF signal always determined the output timing of the C6 time-reference circuit.

Tuning of the synchrotron can result in drifts in the rf-proton phase over extended periods of time, as was discussed in Sec. II A. We set up a balance system consisting of the rf pulse in coincidence with each of two pulses from the γ -ray telescope, one slightly too early and the other slightly too late. The fine delay of the rf signal ahead of all our circuitry was adjusted manually to maintain equality of the two coincidence rates. The timing was maintained by this procedure during periods between actual time-calibration runs of the K detector. The sensitivity of the balance system was better than 0.1 nsec. Adjustments of the delay by amounts greater than 0.2 nsec were rarely necessary.

E. Miscellaneous

1. Data Taking

The data were usually taken in runs of standard length, each run corresponding to a given detector position and to some set of neutral beam conditions.

Each standard run proceeded to an Awschalom monitor count of 4×10^6 , consuming typically 90 minutes, whence automatic type and paper-tape punch equipment recorded the analyzer spectra, the contents of several scalars, and identification information. Photographs of oscilloscope displays of the spectra were also taken. Bookkeeping and rough data analysis were performed with the aid of an IBM 1620, usually within a few hours of a run. Timing-calibration runs of somewhat shorter than standard length were taken using electron pairs as described in Sec. II D, typically once in 12 h. Background runs, to be discussed shortly, were also taken.

All data were taken with the center of the detector ≥ 26 ft from the internal target. This minimum distance was chosen to ensure that the fringe field of the second magnet did not affect the detector efficiency (cf. Fig. 2).

The K_2^0 - p total cross-section measurements were made using the method of C- CH_2 difference; that is, alternate runs were taken with carbon and polyethylene targets, respectively, placed in the beam, and the ratios of the counting rates for each K_2^0 flight time were compared to yield the attenuation of K 's with that flight time by hydrogen. Use of a liquid-hydrogen target of a size which would have fit into the experimental geometry (cf. Fig. 2) would not have improved the statistical accuracy of the measurements appreciably. Each target contained ten blocks and each C- CH_2 pair of blocks was matched so as to contain the same amount of carbon. The C blocks were spaced so that the over-all lengths of the two targets were the same. The carbon target amounted to $\sim 1\frac{1}{2}$ mean free paths, and the hydrogen portion of the polyethylene to ~ 0.2 mean free paths, at 250 MeV/c, a typical K momentum. During the course of the experiment, 13 runs with carbon and 16 with polyethylene were taken. This gave about 7×10^4 total counts in the momentum range of 160 to 350 MeV/c. Attenuation measurements for the heavy elements were made using the method of com-

TABLE II. Target parameters.

Target	Length (in.)	g/cm^2	$(1/\rho L)$ (mb) ^a assuming 100% purity	Purity
CH_2	40 ^b	95.80 ± 0.10	242.7 ± 0.3	$>99.97\%$
C	40 ^b	82.03 ± 0.15	242.9 ± 0.4	$>99.92\%$
Be	8.62 ^c	47.08 ± 1.87	318 ± 12	98.3%
Al	12	84.26 ± 0.62	531.4 ± 3.9	92.5% ^d
Fe	12	238.7 ± 1.1	388.5 ± 1.8	98.6%
Cu	9.59 ^e	216.9 ± 1.0	486.4 ± 2.3	$>99.90\%$
Pb	8	225.8 ± 0.7	1523.5 ± 3.6	98.4%
U	4	187.8 ± 4.6	2105 ± 51	*

^a Inverse of the number of particles per unit area. A "particle" is a primitive CH_2 group in the case of CH_2 .

^b Constructed in the form of 10 blocks. The carbon blocks were spaced with 2-in. gaps.

^c All targets were 4 in. \times 4 in. in cross section except for Be and Cu. The Cu was a 2 $\frac{1}{2}$ -in.-diam cylinder, set in polyurethane support. The Be was composed of a square block and several disks set in polyurethane support.

^d The principal impurity in the Al target was Cu, 4.3% by weight.

^e The uranium was obtained from Oak Ridge National Laboratory. We have assumed it to be pure U^{238} .

paring rates with target in to rates with target out. These measurements consumed an equivalent of 18 standard runs in total. All cross-section data were taken at the 26-ft position. All cross-section targets were measured, weighed, and spectroscopically analyzed. Some relevant parameters for the various targets are listed in Table II.

Data taken for the purpose of measuring the K_2^0 mean life were taken in four series. Each series consisted of four standard runs with the detector at 26, 31, 36, and 41 ft, respectively. A series, together with peripheral runs and synchrotron down time, consumed typically 13 h. The attenuation due to decay in flight over each 5-ft step was, e.g., 18% at 250 MeV/c.

Time spectra taken with the detector at 26 ft with no target, C target, and CH₂ target, respectively, are shown in Fig. 8. Backgrounds, to be discussed shortly, are also shown. The normalization is the same for all curves.

2. Backgrounds

Ghosts. Flight times at the PPA are measured modulo (proton bunch spacing) as we remarked in the Introduction. In our case this spacing was ~ 67 nsec. Thus the K mesons can be classified according to the ~ 67 -nsec time periods into which their flight times fall. We define the periods so that the early end of the first period is the flight time of a particle traveling with the speed of light. The second period begins ~ 67 nsec later in flight time, the third ~ 134 nsec, and so on. The measured spectrum is the superposition of all periods. In our case the maximum of the true K spectrum fell in the first period. Therefore we define "good" events to be those with flight times in the first period. Events with flight times in the other periods, called "ghosts," were treated as background.

The ghosts in the second period were measured in the following manner: The chopper circuitry was modified (cf. Sec. II A) to give a bunch spacing of ~ 134 nsec. A data run of length about $1\frac{1}{2}$ standard runs was taken with the detector at 31 ft and with appropriate adjustments made to the timing system. The late half of the resulting spectrum comprised the ghosts in the second period during normal running, neglecting still later periods. The ghost spectrum, corrected to 26 ft and with background subtracted, is shown in Fig. 8. It is seen to be small, of order 1% or less of the spectrum with no targets, for "real" K momenta below about 400 MeV/c. This is because of the reduced production spectrum and because of the greater attenuation due to decay in flight from the internal target, for kaons with very low momenta. Clearly, ghosts in higher periods may be neglected.

Alternate-bunch contamination. The chopping system which produced the ~ 67 -nsec internal beam structure (see Sec. II A) did not function perfectly and there was generally some amount of internal beam in the wrong set of phase-stable regions. This gave rise to the same

effects as would ghosts (in the above sense) at ~ 33 -nsec intervals during unchopped operation, except that the ghost fraction was diluted by a factor which is the ratio of the beam in the wrong bunches to that in the right bunches. This ratio was measured after each K data run by analyzing the time distribution of counts in the γ -ray telescope for two to three minutes. The γ 's produced by the wrong groups of protons appeared as a small satellite peak, displaced from the main peak by ~ 33 nsec. The sensitivity of the ratio measurement was better than 5×10^{-4} . The percentage contamination in the wrong bunches was quite small; it averaged 0.2% during the lifetime measurement, 0.4% for the C-CH₂ runs, and 0.2% for the heavy elements.

Plug-closed background. Background not associated with the neutral beam was measured by inserting the Pb plug situated on the target table (cf. Fig. 2) into the beam line. The amount of Pb was 3 ft along the beam. The resulting spectrum, with the detector at the 26-ft position, is shown in Fig. 8. It constituted the major contribution to the background given in Table I. Plug runs of standard length were taken periodically throughout the experiment. They were taken at all four detector positions during the lifetime measurement.

The pronounced time structure (cf. Fig. 8) of this "plug-closed" background may be of interest to other experimenters using the PPA. If the background were caused by high-energy neutrons coming through the shielding wall more or less directly from the internal target, then we would expect the detected spectrum to fall off below ~ 300 – 400 MeV/c, as seems to be the case, both because of the character of the neutron spectrum at wide angles¹⁴ and because of threshold effects in the detector. However, we have no explanation of the peak which occurs at long flight times. We determined that the background was not due to accidental coincidences. Its cosmic-ray contribution was 15% and was uniform in apparent flight time. We tested the possibility that the background originated from particles traversing cracks in, or otherwise getting around, the beam plug by taking a run with the plug in the beam and with additional plugging of the beam inside the exit end of the collimator. There was no change in the total rate, at the significance level of 3%. There was also no decrease in the total rate with plug in, at the significance level of 7%, when the secondary beam of our nearest-neighboring experiment²¹ was closed. The spectra of plug runs taken at each given detector position were stable, within statistics, through the data-taking period.

Other background. The above three types of background were easily measured and corrections for their presence could be made to the data in a straightforward manner. Some additional beam-associated background was also present. This background was not directly measured, but was inferred from consistency checks in

²¹ L. B. Auerbach, J. MacG. Dobbs, A. K. Mann, W. K. McFarlane, D. H. White, R. Cester, P. T. Eschstruth, G. K. O'Neill, and D. Yount, Phys. Rev. **155**, 1505 (1967).

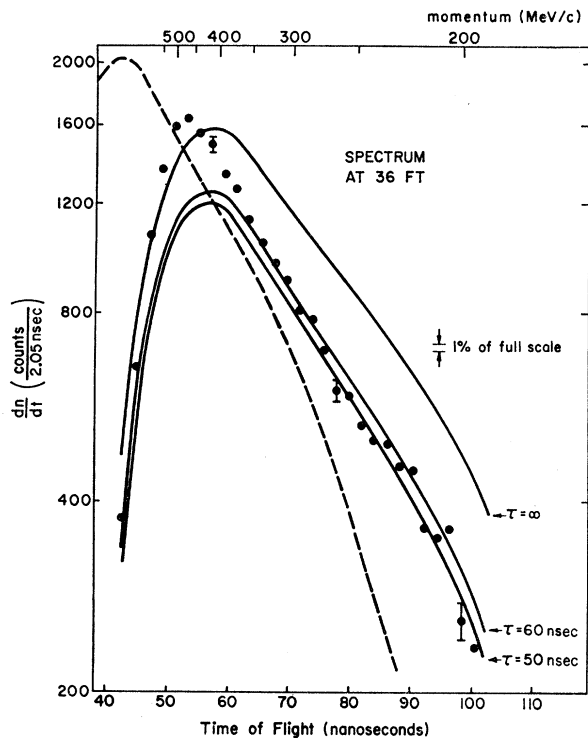


FIG. 9. Measured time spectrum at the 36-ft position with no targets. The dashed curve is the corresponding spectrum at 26 ft. The solid curves are the spectra expected at 36 ft for various values of the K_2^0 mean life, generated from the 26-ft spectrum. The data shown are one-half of the total available data at 36 ft.

the data analysis. The procedure for determining this background is described in Sec. III C. For the moment it will suffice to say that its amount depended upon K momentum and varied between 0 and 4% of the spectrum with no targets, for momenta below about 350 MeV/c.

3. Internal Consistency

We display in Fig. 9 the results of some preliminary data analysis which was performed during the running of the experiment and which gave us indication of the extent to which the apparatus functioned properly. The points are the detector spectrum at the 36-ft position. The solid curves are those expected for various values of the K_2^0 mean life. They were generated from a similar spectrum at 26 ft (the dashed line), taking into account the ghost and plug-closed backgrounds. It is obvious from inspection of the figure that particles with mean life $\sim 5-6 \times 10^{-8}$ sec were indeed detected in a reasonably well-understood manner, for K momenta below about 350 MeV/c. For higher momenta, this was not the case. We believe the discrepancies at higher momenta to have been caused by a background of neutron-induced events in the vicinity of the detector, the neutron source having been neutrons scattered out of the beam at the collimator exit. The discrepancies at high momenta in this consistency check and in others

were sufficiently large that we did not feel justified in attempting to analyze the data in that region. Only data for momenta below 360 MeV/c are considered in the remainder of this paper.

III. DATA ANALYSIS

We describe the analysis of the data in this part of the paper. In Sec. III A, we discuss in detail the determination of precise K_2^0 momenta from the observed pulse-height analyzer spectra. The determination of K_2^0 total cross sections from purely statistical analysis of the attenuation measurements is discussed in Sec. III B. Corrections to these results are discussed in Secs. III C and III D. Finally, we discuss the analysis of the K_2^0 mean-life measurement in Sec. III E.

A. Determination of Momenta

“Nominal” K_2^0 flight times were defined in a straightforward manner as follows: First, the spectra for the various data runs with given detector and neutral beam conditions were shifted so that the analyzer scale positions of the electron peaks obtained from the corresponding timing runs all coincided. It was assumed that the resulting peak position referred to the geometric center of the detector; that is, that all $\beta(=v/c)=1$ particles reaching the geometric center would produce counts at that peak position. Call the peak position C_0 in units of analyzer channels. The nominal flight times, velocities, and momenta, respectively, for events stored in channel C were then calculated from

$$t = L/c + (C - C_0)/X, \quad (2)$$

$$v = L/t, \quad (3)$$

$$p = mv(1 - v^2/c^2)^{-1/2}, \quad (4)$$

where L is the distance from the target to the center of the detector; c is the speed of light, 0.9836 ft/nsec; X is the analyzer scale factor, 1.937 channels/nsec, determined as described in Sec. II D; and m is the K mass, 497.8 MeV/c².

The above nominal kinematic quantities are not precisely equal to the corresponding real quantities for two reasons: (1) “smearing” caused by the finite resolution of the timing system; (2) some calculable corrections to the assumptions used in finding the nominal quantities. In addition there may have been errors in the time measurements. In the case of the total cross-section measurements, such effects would primarily alter the apparent functional dependence of the cross section for a given element upon momentum. They affect the mean-life measurement in somewhat different fashion. As will be seen, the corrections and possible timing errors appeared to be quite small in the case of our experiment. We discuss these effects in the remainder of this section.

The time resolution function consisted of contributions from: (1) geometric effects caused by finite

TABLE III. Timing effects.

1 Nominal momentum (MeV/c)	2 Time resolution (nsec FWHM)		3 FWHM momentum resolution		4 Flight-time correction (nsec)		5 Corrected momentum (MeV/c)	6 Correction to mean life (%)
	Geometric	Total	(MeV/c)	(%)	Geometric	Total		
342	0.4	3.6	39	11	0.17	-0.13	343	...
307	0.8	3.6	31	10	0.12	-0.16	308	...
280	1.2	3.7	26	9	0.10	-0.20	281	-0.4
257	1.6	3.8	22	$8\frac{1}{2}$	0.09	-0.22	258	-0.2
238	1.8	3.9	19	8	0.08	-0.23	239	0.0
222	2.1	4.1	17	$7\frac{1}{2}$	0.07	-0.26	223	0.0
208	2.3	4.2	15	7	0.06	-0.26	209	0.0
196	2.4	4.3	14	7	0.06	-0.27	197	0.2
186	2.6	4.4	12	$6\frac{1}{2}$	0.05	-0.27	187	0.3
176	2.8	4.5	11	$6\frac{1}{2}$	0.05	-0.28	177	...
167	2.9	4.5	10	6	0.04	-0.28	168	...

detector size; (2) jitter in the electronics; (3) the finite proton bunch width (~ 0.7 to 1.1 nsec as discussed in Sec. II A); and (4) the residual rf timing variation over the target spill (about 1 nsec as discussed in Sec. II D). The resolution function was presumably just the shape of the peak obtained in the timing calibration runs except for differences in the geometric effects corresponding to K decay products and electron pairs, respectively. This peak was asymmetric and fit well to a Gaussian with different half-widths on the two sides; the "early" (i.e., short flight time) and "late" half-widths at half-maximum were 1.5 and 2.1 nsec, respectively. This skewness was characteristic of the K detector itself, not of the synchrotron, because a similar effect did not appear when analyzing the γ -ray telescope. We have assumed the skewness, as well as other electronic effects, to be the same for K decay products as for e pairs. We estimate the possible timing error caused by these assumptions to be ± 0.1 nsec, assuming the reasonable hypothesis that such effects resulted from the different time slewing in the primary discriminators caused by differences in the pulse heights of signals which originated in various parts of the counters. The width of the e -pair peak was reasonably stable, varying by about 10% during the course of the experiment. The half-widths which are quoted above and which are used in the following were the largest observed values.

The time resolution functions corresponding to geometric effects alone were calculated for both K 's and e pairs, in order to correct the empirical function to yield the resolution for K 's. In the case of e pairs, under the approximation that the irradiation of the counters is uniform and that the e^+ and e^- positions at the counters are uncorrelated; neglecting motion of the particles and of the light in the scintillation plastic transverse to the beam line; and with the lightpipes pointing downstream (cf. Sec. II C); then the "geometric" time distribution is a saw-tooth function with full width $(n-1)D/c = 1.2$ nsec, where n is the index of refraction of the plastic and D is the length of the counters. The stated approximations were adequate in our case. The corresponding time distribution for K

decays at given momentum is not so transparent and was calculated for each of several momenta using a Monte Carlo program (the program is discussed in Sec. III E). The functions were well approximated by Gaussians. The widths were calculated, using interpolation for some momenta, and are given in column 2 of Table III. The empirical function obtained with e pairs was corrected for each K momentum by subtracting and adding the e pair and K decay geometric contributions, respectively. For this purpose all distributions were approximated by Gaussians; the additions and subtractions were performed using sums of squares; and the early and late half-widths were treated separately. The results for the total time resolution widths corresponding to the detection of K_2^0 particles are given in column 3 of Table III. The corresponding momentum resolution widths, with the detector at 26 ft from the internal target, are given in columns 4 and 5 and also in Table I. For other detector positions, the momentum resolution width scales as the inverse of the target-to-detector distance.

The momentum dependence of the momentum resolution given in Table III is essentially governed by two effects: (1) For constant time resolution, the percentage momentum resolution deteriorates at high momenta because of the relativistic velocity limit. (2) The time resolution in our case was narrower for increasing momentum, thus tending to compensate for the first effect. The reason for the latter effect is as follows: The light in the scintillation plastic and the K mesons both traveled downstream along the beam, the light having a larger velocity ($\beta_P = 1/n = 0.63$) than that of the K 's in the useful momentum region ($\beta_K < 0.6$). Thus decay vertices at different points along the beam, but with the same decay configuration, would produce counts at slightly different times. The full time spread would be largest for the greatest mismatch of velocities, hence it would be a decreasing function of momentum. This elementary approach yields a time spread of $(D/c)(1/\beta_K - n)$, which predicts numbers very close to the Monte Carlo results in column 2 of Table III. However, the over-all time resolution was largely dominated

by the momentum-independent nongeometric effects, as is seen by comparing columns 2 and 3. Thus the momentum dependence of the system momentum resolution was primarily determined by the relativistic effect [effect (1) above].

One other momentum-dependent resolution effect may be mentioned. As was discussed in Sec. II D, the change in rf and in the rf-proton relative phase during the target spill can cause variations in the time comparison of the rf signal with signals produced by monochromatic secondary particles. One can partially compensate for these effects, as we did, by adjusting the delay in the rf signal used for timing. However, one can do so, strictly, only for particles with a definite flight time. The residual timing variations across the spill will be slightly different for different flight times. This difference may be estimated from the time dependence of the rf and is less than 0.3 nsec for our flight-time interval of 67 nsec. Thus the contribution to the width of the time resolution function due to the residual timing variation alone was different for K 's of different momenta by an amount which was less than 0.3 nsec out of an average effect of order 1 nsec. Since the complete time resolution width was of order 3 nsec, it is clear that this "nonmonochromatic" effect may be neglected, and we have done so.

We next discuss systematic effects which necessitated corrections to the nominal times defined by Eq. (2). First, there was an effect caused by referring the timing to the geometric center of the detector: The average e pair produced a count at the same time as would have a $\beta=1$ particle striking a counter, not at the center, but slightly upstream of center. The average K of given velocity also produced a count at the same time as would have a particle with that velocity striking upstream of the center, but by a different amount. This difference gives the correction to be applied to nominal timing. According to the saw-tooth function mentioned previously, the e pairs counted *later*, on the average, than was assumed nominally by $(n-1)D/6c=0.2$ nsec. The time shifts corresponding to K detection were obtained from the same Monte Carlo time distributions as were used to determine the resolution (see above). The differences between these K shifts and the e -pair shift were taken. The resulting geometric corrections to the time calibration are given in column 6 of Table III. The sense is such that real times are greater than the corresponding nominal times. These geometric corrections are quite small, generally less than 0.1 nsec.

There were also time shift effects associated with the "binning" of the data and with the finite resolution, in conjunction with the shape of the K_2^0 time spectrum. Such effects are normally miniscule but were somewhat aggravated in our case because of the asymmetry of the resolution function. The shifts were calculated by folding the momentum-dependent time resolution functions discussed earlier into a hypothetical "real" spectrum, varying this spectrum in such a way as to reproduce the

observed spectrum, and then by comparing the real average flight time for each given group of data with the nominal average. With a spectrum decreasing with flight time (cf. Fig. 8 to the right of the peak) and with a resolution skewed toward later times, one would expect that the real times would be less than the corresponding nominal times. This was the case, and the time shifts were typically $\frac{1}{4}$ nsec. It was verified that the spectra for different cross-section targets at the 26-ft detector position were sufficiently similar in shape that the time shifts for given momenta were the same to within 0.1 nsec. It was also verified that the grouping of data into bins of width up to the resolution width, as was done in the data analysis, caused no effects upon the time shifts, to within 0.1 nsec.

The total time correction, i.e., the sum of the geometric and skewing effects, is given as a function of momentum in column 7 of Table III. The correction is less than 10% of the corresponding resolution width in each case. The corrected momenta are given in column 8 with the corresponding nominal momenta in column 1. The momenta quoted are the averages over those 7-channel bins which were actually used in the cross-section data analysis. The correction is about 1 MeV/ c in each case.

It was convenient in the case of the analysis of the K_2^0 mean-life data to compare counting rates at different detector positions for the same nominal velocity (see Sec. III E). Corrections to nominal timing were considered *a posteriori*. The correction procedure was as follows: The time resolution and the geometric time-shift effects discussed above were applied to a hypothetical "real" K spectrum which was varied until the observed spectrum in nominal time, with the detector at one position, was reproduced. This real spectrum was propagated to the other detector positions, assuming the result of the statistical data analysis for the K_2^0 mean life. Spectra in nominal time at these other positions were also generated by applying the resolution and shift effects. A fictitious data analysis which duplicated the actual analysis procedures for the mean life (Sec. III E) was then applied to these generated nominal spectra. Fictitious mean lives were thus calculated for various intervals of nominal momenta. The correction to the mean life for each such interval was then obtained by comparing the corresponding fictitious mean life with the mean life which was used to generate the spectra. The results are given in column 9 of Table III for the momentum range used in the mean-life measurement. They are expressed as percent corrections to be applied to the mean life obtained from the purely statistical analysis of Sec. III. The effects are quite small and have different algebraic signs. A weighted average of the corrections over momentum was taken. The resulting net correction to the K_2^0 mean life is 0.0% of its value with an estimated uncertainty of 0.2%. This correction and its uncertainty are negligible in comparison with the purely statistical error (about 2.5%) in the mean life.

We have investigated the possibility of systematic errors in the time measurements, as follows. Timing errors may be conveniently categorized into "absolute" and "relative." By "absolute error," we mean an overall shift in time of the pulse-height analyzer scale. Such shifts could have arisen from the following sources: (1) The uncertainty in the corrections to the time calibration which were discussed earlier is about ± 0.1 nsec. (2) The average scintillation-counter pulse heights produced by K decay products and by the e pairs used for time calibration, respectively, could have induced different time slewing in the primary discriminators by about 0.1 nsec. (3) There were timing fluctuations in the K detector of ~ 0.1 – 0.2 nsec caused by certain instabilities in the photomultiplier high-voltage distribution system; they most likely were absorbed into the time resolution function, but perhaps could have been correlated with detector position and/or with neutral beam conditions. (4) The positions of the time-calibration peaks were visually located to ± 0.1 nsec; they also could conceivably have been correlated with the running conditions for neighboring data runs. Including all of these effects, we estimate the uncertainty in the absolute position of the analyzer time scale to have been ± 0.25 nsec.

By "relative error," we mean an error in the timing of a K with some given momentum relative to the timing of a K with $\beta=1$. Such errors could have been caused by an error in the analyzer channels-to-time conversion factor and/or by nonlinear distortions of the scale. From the known limits on these effects (see Sec. II D), we estimate the maximum relative error to be a function of momentum which varies roughly linearly between 0 at the $\beta=1$ position to 0.2 nsec at a position 67 nsec later in flight time.

The following effects have also been considered as possible sources of timing error, are estimated to contribute less than 0.1 nsec each, and have been neglected: (1) drifts in the Chronetics circuits; (2) differences in rate-induced time slewing in the ac-coupled logic circuitry caused by differences in total counting rate during data runs and time-calibration runs, respectively; (3) errors in the position of the detector; (4) electrons used for the timing runs having velocities $< c$; (5) the possibility that the average K with a given momentum occurred at a different time during the spill than did the average K with a different momentum, or than did the average e pair used for calibration, correlated with the different rf timing through the spill; (6) errors in the delays of the RG8U cables which were used to compensate for changes in detector position; and (7) residual drifts in the rf timing averaged over the spill.

The timing uncertainties discussed above (0.25 nsec absolute, typically 0.1 nsec relative) are comparable in magnitude to the corrections to nominal timing which are listed in Table III. Thus the average momentum for any group of K 's is known to about 1 MeV/ c , and in

every case the uncertainty is less than 10% of the resolution width.

The effect of the absolute scale position uncertainty upon the mean-life measurement was estimated by a procedure similar to that used to estimate the resolution and time correction effects (see above): The procedure was the same except that extra 0.25-nsec time shifts were inserted at appropriate stages. The resulting uncertainty in the mean life, after averaging over momentum, is $\pm 0.2\%$ of its value. The effect of possible relative timing errors would have been to cause the counting rate at one analyzer scale position and for one detector position to be compared with the counting rate for another detector position at a slightly wrong scale position. This is because the scale positions for given K velocity were different for the various detector positions except in the case $\beta=1$. Thus such effects are in general dependent upon the shapes of the spectra. (To some extent, wrong comparisons of counting rates would also have been produced by absolute errors; any such effects were automatically included in the procedure mentioned above.) An estimate of the effects caused by possible relative time errors was made by assuming a relative error which varied between 0 and 0.2 nsec across the time scale (the maximum error estimated previously) and by distorting the scale accordingly. Averaged over the appropriate momentum region, the resulting uncertainty in the mean life is $\pm 0.3\%$. This uncertainty and the 0.2% uncertainty due to the absolute effect are negligible in comparison with the statistical error.

In summary, we measured individual K_2^0 momenta with our timing system to an accuracy which was limited essentially by a momentum resolution function whose width varied between 6% and 12% (FWHM), with the detector at 26 ft from the internal target (for example), over the momentum range 160–350 MeV/ c . The effects of all timing uncertainties upon the measurement of the K_2^0 mean life were negligible.

Finally, we have verified by direct velocity measurement that the relativistic limiting speed for electrons is indeed the speed of light, to about $\frac{1}{2}\%$. Our result is

$$1 - v_{\max}/c = 0.005 \pm 0.005. \quad (5)$$

This followed in straightforward fashion from comparison of e -pair calibration runs taken at two detector positions separated by 15 ft with the lead radiator fixed at the collimator exit. The quoted uncertainty is dominated by the uncertainties in the delays of the RG8U compensating cables.

B. Total Cross Sections, First-Stage Analysis

The attenuation of the momentum spectrum by various absorbers was measured during this experiment. For "ordinary" particles, such attenuation measurements yield total cross sections in a straightforward manner, as is well known. However, the peculiar nature of neutral kaons gives rise to a small nonlinear depen-

dence of the absorption length upon density. We discuss this effect first, and the actual data analysis later in this section [after Eq. (13)].

Consider some definite value for the momentum and some definite absorber. The attenuation of a K_2^0 beam by the absorber is then given, to a good approximation, by²²

$$I(L)/I(0) = \exp[-\rho L(\sigma_2 + \rho\zeta) - t/\tau_2], \quad (6)$$

where ρ is the absorber particle density; L is the length of the absorber; σ_2 is the K_2^0 "total cross section" [see Eq. (9) below and the comments which follow it] appropriate to the absorber and momentum; t is the time taken for a K_2^0 to traverse the distance L , measured in the K rest frame; τ_2 is the K_2^0 mean life; and $I(0)$ and $I(L)$ are the intensities at the entrance and exit of the absorber, respectively. The quantity ζ is given by

$$\zeta = 2\lambda^2\beta\gamma c\tau_1 \operatorname{Re}\{[f_{21}(0)]^2/(\frac{1}{2} - i\delta)\}, \quad (7)$$

where λ is the de Broglie wavelength in the laboratory frame; βc is the K_2^0 velocity; $\gamma = (1 - \beta^2)^{-1/2}$; τ_1 is the K_1^0 mean life; δ is the K_2^0 - K_1^0 mass difference (positive if the K_2^0 is the heavier) in units of $\hbar/\tau_1 c^2$; and

$$f_{21}(0) = \frac{1}{2}[f(0) - \bar{f}(0)], \quad (8)$$

where $f(0)$, $\bar{f}(0)$ are the forward elastic scattering amplitudes for K^0 and \bar{K}^0 , respectively. Furthermore, the parameter σ_2 is given by

$$\sigma_2 = \frac{1}{2}(\sigma + \bar{\sigma}), \quad (9)$$

that is, the average of the K^0 and \bar{K}^0 total cross sections. It is easy to show that this σ_2 is indeed the K_2^0 total cross section, i.e., the result of summing the K_2^0 -nuclear interaction over all final states. Thus Eq. (6) contains, in addition to the normal terms describing nuclear absorption and the decay of an unstable particle, an extra term in the exponent. This term ($\rho^2\zeta L$) is a quantum-mechanical effect which is peculiar to neutral kaons and which is generally quite small. Equation (6) may be derived by a Huygens-wave calculation of the propagation of K_1^0 and K_2^0 mesons through matter, taking into account the coupling between the two states, with suitable approximations. We refer to the term nonlinear in ρ as the "density effect."

In our experiment, what was actually measured was the ratio of K_2^0 intensities for two different absorbers (targets), or for one absorber and for vacuum. This of course removes the decay-in-flight term in Eq. (6) from consideration: Applying Eq. (6) to the case of no target over some beam length, so that $\rho = 0$, and dividing the result into the same equation applied to some target labeled A of equal length, we get

$$I^A(L)/I^0(L) = \exp[-\rho^A L(\sigma_2^A + \rho^A \zeta^A)], \quad (10)$$

where the superscript 0 refers to the intensity with no target. The intensity ratio is the same at any point

downstream of the position of the target, and we may suppress the dependence of the ratio upon L . For a carbon-polyethylene difference experiment with matched targets (i.e., $\rho^C L^C = \rho^{\text{CH}_2} L^{\text{CH}_2}$), the corresponding result is

$$I^{\text{CH}_2}/I^C = \exp\{-\rho^{\text{CH}_2} L^{\text{CH}_2}(2\sigma_2^{\text{H}} + \rho^{\text{CH}_2} \zeta^{\text{CH}_2} - \rho^C \zeta^C)\}, \quad (11)$$

where σ_2^{H} is the K_2^0 - p total cross section and where we have used $\sigma_2^{\text{CH}_2} = \sigma_2^{\text{C}} + 2\sigma_2^{\text{H}}$. The carbon cross-section term cancels, as is normal with matched targets, but the density effect term does not. The quantity ζ^{CH_2} in Eq. (11) may be found by substituting $f^{\text{CH}_2}(0) = f^{\text{C}}(0) + 2f^{\text{H}}(0)$ (which follows from the superposition principle), and a similar expression for $\bar{f}(0)$ into Eq. (8), and then the result of Eq. (8) into Eq. (7). The resulting object ζ^{CH_2} is not a simple sum of carbon and hydrogen effects; thus it is more proper to think of it as being a property of the CH_2 molecule.

The ζ parameters in Eqs. (10) and (11) depend, through Eqs. (7) and (8), upon K -nuclear forward scattering amplitudes which are not known for low K momenta. However, they can be estimated fairly reliably from nuclear models²² which have given a good account of the interactions of charged kaons in nuclear emulsion.²³ We have estimated the ζ parameters for the molecules appropriate to our experiment after the method of Ref. 22. We find that the extra terms in Eqs. (10) and (11) are quite small in comparison with the corresponding σ terms. Specifically, the best estimates are

$$|(\rho^{\text{CH}_2} \zeta^{\text{CH}_2} - \rho^C \zeta^C)/2\sigma_2^{\text{H}}| \lesssim 0.015 \quad (12)$$

and

$$|\rho^A \zeta^A/\sigma_2^A| \lesssim 0.005 \quad \text{for all } A. \quad (13)$$

These effects are also small in comparison with our experimental errors in the total cross sections. Therefore we have neglected the density-effect terms.

With the neglect of the density effect, we may solve Eqs. (10) and (11) for the total cross sections in terms of experimentally measured quantities, obtaining well-known expressions. We introduce the specific number of detector counts (N) for the target and momentum interval in question and normalize to the number of counts (M) in the Awschalom monitor (described in Sec. II B). We also allow for background subtraction (superscript B in the following). The resulting equations to be used in obtaining the K_2^0 - A and K_2^0 - p total cross sections are, respectively,

$$\sigma_2^A = \frac{1}{\rho^A L^A} \ln\left(\frac{N^0/M^0 - N^B/M^B}{N^A/M^A - N^B/M^B}\right), \quad (14)$$

$$\sigma_2^{\text{H}} = \frac{1}{2\rho^{\text{CH}_2} L^{\text{CH}_2}} \ln\left(\frac{N^{\text{C}}/M^{\text{C}} - N^B/M^B}{N^{\text{CH}_2}/M^{\text{CH}_2} - N^B/M^B}\right), \quad (15)$$

²² E. F. Beall, Phys. Rev. 152, B1486 (1966).

²³ B. Sechi-Zorn and G. T. Zorn, Phys. Rev. 120, 1898 (1960).

with obvious notation. We have assumed the background to be independent of target condition in the above expressions, as only the background measured with the beam plugged (cf. Sec. II E) was considered in the first-stage analysis. The other backgrounds will be discussed later.

The first stage of the cross-section analysis proceeded by applying Eqs. (14) and (15) to the data. The analyzer spectra were divided into flight-time bins of 7 channels, corresponding to ~ 3.5 nsec, in width. This was approximately the resolution width. The upper and lower momentum cutoffs were 360 and 165 MeV/ c , respectively (cf. Figs. 8 and 9). Division of the data was also made into that recorded by the different sets of counter-telescope combinations (AC, BD and the adjacent pairs were recorded separately, see Sec. II D).

The C-CH₂ data were examined for internal consistency prior to the actual calculation of total cross sections: The attenuation due to hydrogen, averaged over momentum, was calculated for each of 14 pairs of runs distributed over the experiment. The standard deviation in each resulting number was 2.0% of its value. The χ^2 for deviation of these numbers about a common mean was 11.7 for 13 degrees of freedom, yielding a χ^2 probability of 55%.

The numbers of counts N^A , N^0 , and N^B in Eq. (14), or N^C , N^{CH_2} , and N^B in Eq. (15) were independently measured and thus the standard deviations in sums and differences of them may be estimated using Gaussian statistics. To calculate the errors in the cross sections, we have also used the approximations that the logarithms in Eqs. (14) and (15) are Gaussian-distributed in the counting rates. That is, we used

$$d\sigma(N_1, N_2, N_3) = \left[\sum_{i=1}^3 \left(\frac{\partial \sigma}{\partial N_i} dN_i \right)^2 \right]^{1/2}, \quad (16)$$

with

$$dN_i = \sqrt{N_i}, \quad (17)$$

where the sum is over target, vacuum, and background in the case of Eq. (14), or over C, CH₂, and background in the case of Eq. (15). The statistical errors in the monitor numbers were negligible.

The results of the first-stage calculation of the K_2^0 - p total cross sections are given in Table IV. The quoted momenta are the average values over the respective bins, corrected as described in Sec. III A.

It is seen by inspection of Table IV that there are systematic differences between the cross sections corresponding to the various telescope combinations. The results for the adjacent pairs are lower than those for the BD (horizontal) pair by $25\% \pm 7\%$ when averaged over the entire momentum range given. Similarly, the AC (vertical) pair gives lower results than does BD by $32\% \pm 7\%$. These "biases" also appear in the case of the heavy elements but are generally smaller. The biases for all of the elements, averaged over the momentum range quoted in Table IV, are given in Table V. The

TABLE IV. First-stage analysis of K_2^0 - p total cross sections. Errors are statistical only.

Corrected momentum (MeV/ c)	Adjacent telescope pairs	Results, in mb, as computed from:			All telescopes*
		AC vertical pair	BD horizontal pair		
343	25.1± 4.1	24.3± 4.3	19.3± 4.4	23.3± 2.5	
308	30.4± 5.0	14.1± 5.1	36.2± 5.1	26.5± 2.9	
281	27.2± 5.3	28.2± 5.6	26.3± 5.7	27.3± 3.2	
258	24.3± 6.3	26.2± 6.1	38.8± 6.6	29.0± 3.7	
239	37.8± 6.9	36.7± 6.9	45.7± 7.4	39.7± 4.1	
223	28.2± 8.7	27.8± 8.3	48.1± 8.1	34.3± 4.9	
209	24.5± 8.6	50.9± 9.0	42.2± 9.1	38.0± 5.2	
197	37.4±12.2	39.9± 9.8	58.5± 9.9	45.0± 6.2	
187	41.7±13.4	35.6±11.6	54.5±11.9	43.4± 7.2	
177	46.9±14.8	40.9±12.5	64.2±13.5	49.9± 8.0	
168	47.0±19.2	46.4±15.2	66.6±16.0	52.6±14.4	

* Computed by first summing the numbers of counts over combinations and then calculating cross sections, rather than by taking weighted averages of the cross sections computed from individual telescope sets. The two methods need not yield exactly the same numbers.

numbers of mean free paths (i.e., $\rho\sigma_2L$, the logarithm of the attenuation), averaged over momentum and over telescope combinations, and the associated statistical errors are also given. Although the biases are not generally great, it is clear that they cannot be considered to be small in comparison with the statistical errors. It is also clear that the anomalous effects are much too uniform in direction to have been caused by statistical fluctuations. Therefore, we found it necessary to correct the results for these anomalies, and this is discussed in the next section.

C. Residual Beam-Associated Background Subtractions

A clue to the nature of the anomalies discussed at the end of the previous section is provided by noticing that the effects in the case of hydrogen are considerably larger than in the case of a typical heavy element (see Table V). The essential difference in experimental conditions was the presence of extra matter in the beam, i.e., the carbon in the C and in the CH₂ targets, in the case of the hydrogen measurement. Therefore it is plausible that the anomalies were caused by the presence of a residual background, in addition to the "plug-closed" background already subtracted, which was attenuated less by matter than were K_2^0 particles, so that the ratio

TABLE V. Cross-section biases. All quantities are averaged over momentum. Errors are statistical only.

Element	$\rho\sigma L$	$(\sigma_{ADJ}-\sigma_{BD})/\sigma_{BD}$	$(\sigma_{AC}-\sigma_{BD})/\sigma_{BD}$
H	0.25±0.01	-0.25±0.07	-0.32±0.07
Be	0.91±0.01	-0.10±0.03	-0.09±0.03
C	1.27±0.01	-0.07±0.01	-0.04±0.01
Al	1.29±0.02	-0.02±0.03	-0.03±0.03
Fe	2.74±0.05	-0.20±0.04	-0.10±0.04
Cu	2.18±0.04	-0.12±0.04	-0.10±0.03
Pb	1.96±0.03	-0.13±0.03	-0.06±0.03
U	1.65±0.02	-0.06±0.03	-0.06±0.03

of background to K 's increased with the amount of matter in the beam and hence caused larger anomalies. There is also some hint of correlation of the biases with respect to the number of mean free paths among the heavy elements (cf. Table V). We made measurements over a considerable range of K_2^0 attenuations and are thus able to show the consistency of this hypothesis of smaller attenuation of the background (in fact zero attenuation), and this will be seen shortly. Further information is available from consideration of the details of the shielding in the neighborhood of the detector; it was such as to shield the various telescopes differently. We have assumed the presence of a background with smaller attenuation than that of K 's and we have performed a least-squares fit at each momentum, with a constraint imposed upon the *ratio* of backgrounds in the horizontal and vertical telescope pairs, to the true cross sections and to the background-to- K ratios for different counter-telescope combinations, using (at each momentum) the first-stage analysis results for the cross sections for *all* the elements as input data. We discuss the details of this calculation in this section.

For purposes of orientation, consider the following model of the background mechanism: A neutron enters the neutral beam collimator (cf. Fig. 2), not necessarily directly from the internal target, and scatters near the exit toward the counters of the detector. The neutron interacts in the wall of the vacuum pipe or in one of the inner counters (cf. Figs. 2 and 3), via an $(n,2p)$ reaction, to produce two charged particles. One of the particles counts in the neighboring counter telescope and the other in a different telescope. If the interaction is near telescope A, for example, then there is some probability that the second particle will count in telescope C. If, on the other hand, the interaction is near B, then the probability of the second particle counting in telescope D is the same as for telescope C in the first case, because of the symmetry of the detector. (Strictly, this statement applies if we take averages of the relevant solid angles over all interaction origins near the faces of telescopes A and B, respectively.) Further, assume left-right and up-down symmetry of all of the matter in the neighborhood of the detector (the most significant violation of this assumption was the iron in the return path of the second magnet which, however, was more than 15 in. away from the center of the beam). Then there would be as many background coincidences in AC caused by an interaction near A as near C, and similarly for B and D. The *ratio* of the numbers of background counts in the AC pair of telescopes to that in BD is then just the ratio of the neutron flux, averaged over some appropriate area, near telescope A to that, averaged over a similar area, near B.

The flux of neutrons at the wall of the vacuum pipe near the counters was attenuated by matter in the region of the second magnet. Specifically, there existed zinc shielding at the sides of the beam line (see Sec.

II B). This zinc was 8 in. in length and 4 in. in width on each side of the beam, and formed a horizontal aperture $4\frac{7}{8}$ in. in width at a point 4 ft downstream of the collimator exit. Geometry then shows that the zinc shielded the B and D (horizontal) telescopes at the median plane from all but a small part of the perimeter of the collimator exit. In contrast, the magnet pole tips formed a vertical aperture of somewhat more than the nominal 6-in. gap width at the same point along the beam, and shielded the vertical counters *only* from a small part of the perimeter. We have approximated the shielding as being only due to the zinc, neglecting the pole tips (and also neglecting the magnet coils, which were further downstream but were still further out of the beam than were the pole tips, and whose average density was considerably smaller).

We have estimated the ratio of AC background to BD background, assuming the above slit-scattering mechanism, using Monte Carlo techniques. Neutron-scattering events in the collimator were generated, were weighted by the appropriate angular distributions, and were followed through the zinc shielding to the detector. The appropriate cross sections and angular distributions were taken from known data.²⁴ Account was taken of diffraction scattering toward the counters as well as absorption. The calculations were performed for neutron momenta between 500 and 800 MeV/c. The lowest momentum value corresponds to the $(n,2p)$ threshold with one proton traversing an entire counter telescope, including the iron absorber (cf. Fig. 3), and the other proton traversing a telescope near its edge where there was a small area not covered by iron (the positioning of the iron is accurately shown in Fig. 3). The AC to BD background ratios obtained ranged from 3:1 and 7:1. Flight-time measurements would yield the neutron momenta only under the assumption that the neutrons came directly from the internal target. We do not believe this to be the case, as will be seen. Therefore we can only say that, considering the momenta of neutrons which were likely to be produced,²⁴ the correct background ratio should lie somewhere between the above two limits, possibly dependent upon K_2^0 momentum. We have assumed an AC to BD background ratio of 5, independent of K_2^0 momentum, for the least-squares fit. This number is our best estimate, and a reasonable estimate of its error would be ± 2 .

Consistent results were obtained from the fit, as will be seen shortly, by assuming that the background underwent *no* attenuation in traversing the cross-section targets. This no doubt means that the background did not traverse the cross-section targets and hence did not come directly from the internal target. With this assumption of zero attenuation, one may easily obtain an expression giving the measured total cross sections obtained from the first-stage analysis in

²⁴ *Neutron Cross Sections*, edited by D. Hughes and R. Schwartz, Brookhaven National Laboratory Report No. BNL 325 (U. S. Government Printing Office, Washington, D. C., 1964), 2nd ed.

terms of the true cross sections and background-to- K ratios. After forming an appropriate χ^2 function, we obtain

$$\chi^2 = \sum_{i=1}^3 \left\{ \sum_{j=1}^7 \left[\sigma_i^{j\text{obs}} - \frac{1}{(\rho L)^j} \ln \left(\frac{1+b_i}{\exp[-(\rho L)^j \sigma^j] + b_i} \right) \right]^2 / (d\sigma_i^j)^2 \right. \\ \left. + \left[\sigma_i^{\text{Hobs}} - \frac{1}{2(\rho L)^{\text{CH}_2}} \ln \left(\frac{1+b_i \exp[(\rho L\sigma)^c]}{\exp[-2(\rho L\sigma)^{\text{CH}_2}] + b_i \exp[(\rho L\sigma)^c]} \right) \right]^2 / (d\sigma_i^{\text{H}})^2 \right\}, \quad (18)$$

where the i sum is over telescope combination sets, and the j sum is over heavy elements; $\sigma_i^{j\text{obs}}$ and $d\sigma_i^j$ (and σ_i^{Hobs} , $d\sigma_i^{\text{H}}$) are the measured total cross sections and associated errors, respectively (given in Table IV in the case of hydrogen); σ^j (or σ^{H}) are the corresponding true cross sections; and b_i is the ratio of background to K rate with no targets in the beam of the i th combination. Other notation is the same as that used in Sec. III B. All quantities in Eq. (18) refer to a given K momentum.

The χ^2 function given by Eq. (18) was minimized separately at each K momentum. The constraint mentioned above, $b_{AC} = 5b_{BD}$, was imposed at each momentum. The results of the fits are given in Tables VI and VII. Table VI gives the fitted background-to- K ratios with targets out, the χ^2 for 14 degrees of freedom, the χ^2 probabilities, and the fitted true K_2^0 - p total cross sections. The quoted errors were determined from the variance matrices. We also give the percentage corrections to the first-stage analysis K_2^0 - p results (see Table IV) which are needed to produce the fitted results. It is seen that the effect of the present procedure is to increase the results for the hydrogen total cross sections by typically 15%. The percentage corrections alone are given in Table VII for the heavy elements. They are generally smaller than in the case of hydrogen, and are typically a few percent (the rather large corrections in the case of iron may be traced to the fact that the iron target contained a greater number of mean free paths, at a typical momentum, than did the other targets). The χ^2 probabilities in Table IV show that the fits are internally consistent.

The corrections at 177 MeV/ c are generally negative, as is the fitted background ratio, averaged over combinations. This would indicate that background at that momentum was actually *created* by the insertion of targets. This is not fundamentally inconsistent as there is some finite error in the assumption of zero attenuation. The other isolated examples of negative corrections in Table VII are due to differences in methods of averaging over telescope combinations; that is, the fitting procedure under present discussion effectively averaged the cross sections over combinations, while the averaged cross sections given in Table IV were computed by summing the numbers of counts, for given beam condition, over combinations prior to calculating the cross sections.

We also made fits without the assumption of zero attenuation in the targets. It was assumed that the attenuation of the background in the targets was determined by known neutron-nuclear total cross sections,²⁴ but multiplied by an efficiency factor which was the same for all elements and combinations (i.e., the attenuation was assumed to be governed by an effective total cross section equal to $f\sigma_n$, where f is the efficiency factor). This factor was allowed to vary during the fit. The results were that the fitted efficiency factor was consistent with zero, within a statistical error of typically 0.1, for all momenta, thus essentially reproducing the constraint of zero attenuation. This means that the zero-attenuation feature is *not* model-dependent.

Measurements taken early in the experiment lend support to the conclusion of zero attenuation. Beam

TABLE VI. Results of residual background fits.

Corrected momentum (MeV/ c)	Background-to- K ratio ^{a,b}		χ^2 ^c	$P(\chi^2)$	K_2^0 - p total cross section ^b (mb)	Correction (%)
	AC	Adjacents				
343	0.053±0.012	0.045±0.012	16.1	32%	26.0± 2.9	11.6
308	0.039±0.015	0.028±0.013	21.3	9%	30.4± 3.5	14.7
281	0.035±0.014	0.046±0.013	11.2	68%	31.0± 3.9	13.6
258	0.026±0.015	0.040±0.014	14.9	39%	33.7± 4.6	16.2
239	0.025±0.014	0.050±0.014	9.8	78%	46.4± 5.5	16.9
223	0.013±0.018	0.024±0.016	21.2	9%	38.5± 6.2	12.2
209	0.000±0.014	0.024±0.016	11.5	66%	41.5± 6.1	9.2
197	0.017±0.015	0.014±0.016	12.3	60%	50.7± 7.8	12.7
187	0.012±0.016	0.033±0.017	6.0	96%	49.0± 9.2	12.9
177	-0.011±0.019	0.008±0.019	6.8	93%	48.7± 9.7	-2.4
168	0.034±0.022	0.064±0.025	9.3	80%	68.3±15.0	29.8

^a This is the fitted ratio of residual background rate to the K rate with only 2-in. Pb in the beam line. The ratio for the horizontal telescope pair (BD) is 0.2 of that for the vertical pair (AC), by hypothesis. The background ratio, averaged over combinations, is the direct average of the three ratios to a good approximation.

^b The quoted errors were determined from the variance matrices of the fit.

^c There were 14 degrees of freedom at each momentum.

TABLE VII. Results of residual background fits.

Corrected momentum (MeV/c)	Correction to cross section (%)						
	Be	C	Al	Fe	Cu	Pb	U
343	5.6	7.7	5.3	21.7	10.6	10.5	8.8
308	3.8	5.3	3.9	16.4	7.0	9.1	5.4
281	5.1	7.1	5.3	24.1	3.9	10.7	7.4
258	4.3	5.7	5.7	8.5	9.4	8.3	6.1
239	5.1	7.0	3.8	19.9	10.9	10.5	7.3
223	1.8	2.6	3.4	15.8	2.4	5.5	2.4
209	1.8	2.4	1.4	1.2	1.2	2.9	2.5
197	2.9	2.7	3.0	11.7	7.8	-0.8	-4.3
187	3.2	4.6	4.3	17.3	-2.6	6.6	3.7
177	0.0	-0.9	-0.8	-1.8	-10.9	-1.6	0.1
168	9.2	7.8	10.6	29.1	17.9	7.2	11.7

profiles were taken with a probe counter with and without the carbon target in the beam. We observed that the tails of the beam profile were attenuated by carbon less than was the umbra region. (We are unable to use this information quantitatively in the present context because this observation was made with a different collimator aperture—a 2.5-in. square—than was used during the data taking; no profiles with the carbon in the beam were taken with the final collimator.)

The model-dependent feature of the fit, namely, the constraint imposed between the AC and BD backgrounds, was studied by varying the background ratio and by observing the resulting effects upon the fitted total cross sections. The changes in the cross sections were typically 1% for a change of the ratio of 2, which is our estimate of its uncertainty (see above). Thus the results are sufficiently insensitive to variations in the model that the fitting procedure seems reasonable. It is true that the results depend upon the fact that we assumed the background to originate in the collimator, in order that use could be made of the ratio of horizontal to vertical shielding; however, if the background did not originate in the collimator (for example, if it were just general leakage through the shielding wall), then it is difficult to understand how it was not subtracted from the original data along with the “plug-closed” background.

Two other possible causes of the anomalies observed in the first-stage analysis remain: (1) Perhaps the “plug-closed” background, which also was asymmetric with respect to the different telescope combinations, was not properly normalized for its subtraction from the data. (2) Perhaps there were efficiency variations in the counters or in the electronics, different for different telescopes, which were correlated with the presence or absence of targets. We can think of no mechanism which would produce the latter effect except for the obvious possibility of rate dependence. This, however, is precluded because of the excellent stability of the detector (cf. Sec. II C). As for the former possibility, (1) the plug background was stable through the data-taking period; (2) different plug runs were used in the subtractions for different groups of cross-section deter-

minations, so that a single “bad” run could not have produced anomalies in all of the results; (3) the effect upon the Awschalom monitor caused by inserting the Pb plug into our neutral beam was estimated and is much too small to account for the sizes of the anomalies; and (4) we have made a thorough search for mistakes in the bookkeeping and have found none.

We have attempted to understand the detailed mechanism of the residual background by independently estimating the background counting rates expected with our detector and beam geometry. These attempts have not been successful. For example, we estimated the absolute background rates as follows: The neutron flux at the detector from collimator slit scattering was estimated, using the known neutron spectrum from the internal target.¹⁴ The background rates in the counters were then estimated using reasonable estimates of the $(n,2p)$ cross sections. The results were at best barely sufficient to explain the fitted backgrounds given in Table VI. However, this calculation assumed that the neutrons came directly from the internal target, whereas it would seem from the lack of attenuation in the cross-section targets, which assumption was necessary in order to fit the data, that the background did not come directly from the internal target. Particle fluxes from the synchrotron which do not come directly from the target should be at least an order of magnitude lower than those that do. Thus this mechanism does not seem to explain all of the facts. Other mechanisms also do not seem to be able to explain the observed effects.

There is no doubt also the possibility that some as yet unknown particle is produced by 3-GeV protons and that these particles produced our anomalies. Such an object would have to have an interaction with matter at least an order of magnitude smaller than that of known strongly interacting particles in order to explain its lack of attenuation in our targets; and it would have to interact with a symmetric detector in an asymmetric fashion in order to produce the observed anomalies. Simplicity and good taste preclude our taking such a possibility seriously. In any case, the effect upon our experiment was that of a background, whatever the source of the background may have been.

To summarize, the only reason we have for doubting the results of the residual background corrections just discussed is that we have not been able to explain them by *a priori* calculations of the background rates caused by known sources. We feel that the fitting procedure itself is sufficiently insensitive to the assumptions which were made that the procedure is valid. We have therefore applied the corrections given in Tables VI and VII to our results for the total cross sections.

The residual beam-associated background just discussed, the “plug-closed” background and the ~ 67 -nsec ghosts were all subtracted in calculating the K_2^0 production spectrum which was discussed in Sec. II C. Their sum is tabulated in Table I.

TABLE VIII. Miscellaneous corrections, in percent, to be applied to the cross sections.

Corrected momentum (MeV/c)	Alternate-bunch effect		H	Be	C	Forward scattering				
	67-nsec ghosts (beryllium)	(hydrogen only)				Al	Fe	Cu	Pb	U
343	-0.6	0.1	0.6	1.5	3.0	0.4	6.3	6.9
308	-0.4	0.1	0.5	1.3	2.2	0.4	5.7	6.0
281	-0.3	0.1	0.5	1.2	1.8	0.3	5.0	5.2
258	-0.2	0.1	0.4	1.2	1.4	0.3	4.5	4.5
239	-0.2	0.1	0.4	1.0	1.3	0.3	3.9	4.0
223	-0.1	0.2	...	0.1	0.4	0.9	1.2	0.3	3.5	3.7
209	...	1.0	...	0.1	0.3	0.8	1.1	0.2	3.1	3.3
197	...	1.6	...	0.1	0.3	0.7	1.0	0.2	2.7	3.1
187	...	2.4	...	0.1	0.3	0.7	0.9	0.2	2.4	2.9
177	...	2.9	...	0.1	0.3	0.6	0.8	0.2	2.1	2.7
168	...	2.6	...	0.1	0.3	0.6	0.8	0.2	1.8	2.6
Impurity correction			...	0.2	...	1.6	0.0	...	-0.8	...
Scale uncertainty			±4%	±4%	±1%	±1%	±2%	±2%	±2%	±3%

D. Further Systematic Effects and Final Results for the Cross Sections

The following further systematic effects in the total cross-section measurements have been considered: (1) forward scattering; (2) ~ 67 -nsec ghosts and alternate-bunch ~ 33 -nsec ghosts (cf. Sec. II E), which were not subtracted in the analyses discussed in the two preceding sections; (3) impurities in the targets and uncertainties in target densities and lengths; (4) the density effect [cf. Eqs. (5)–(12)]; and (5) resolution effects. The density effect was discussed in Sec. III B and is negligible. Resolution effects were essentially taken into account by shifting the time spectra as discussed in Sec. III A. The shifts were the same to an excellent approximation for all spectra taken with the detector at 26 ft, and hence the effects upon the cross sections were negligible. The first three effects above are discussed in the following.

In most transmission experiments a forward scattering correction is necessary because of the fact that some of the particles scattered out of the beam by the target can still reach the detector. In our case this effect was negligible ($< 10^{-3}\%$ for hydrogen, $\sim 0.1\%$ for uranium) because the solid angle subtended by the collimator exit at the attenuation targets was small— 1.65×10^{-4} sr at the center of the target table. However, much larger forward-scattering effects were present in our case because the beam was not collimated at the entrance to the targets; the introduction of a target caused some K 's not originally within the part of the beam defined by the collimator to scatter into that part and to be detected. If the target is small in comparison with the distances involved and if plural scattering may be neglected, then it is easy to show that the correction to the total cross section is

$$\Delta\sigma = \left(\frac{\Omega_{PT}}{\Omega_{PC}} \right) \left(\Omega_{TC} \frac{d\sigma^{el}}{d\Omega}(0) \right), \quad (19)$$

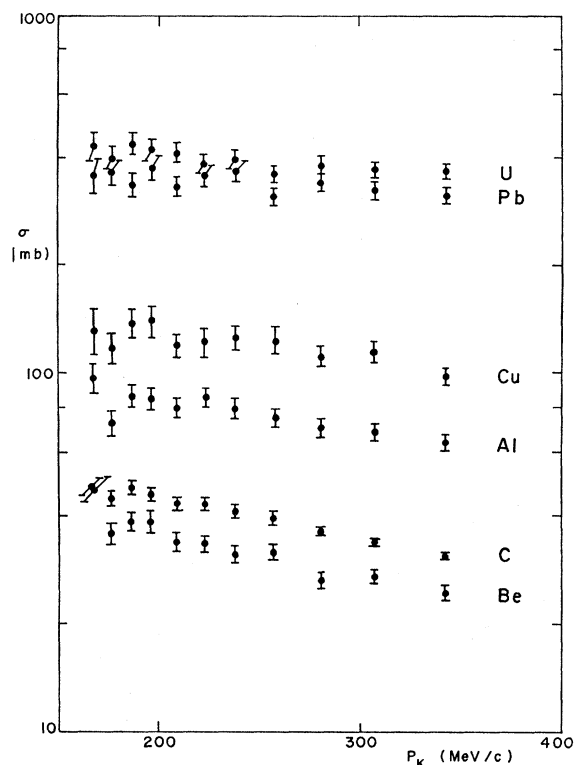
where the subscripts P , T , and C refer to the K_2^0 production point, the target, and the collimator exit, respectively; Ω_{ij} is the solid angle subtended by object j at point i ; and $d\sigma^{el}/d\Omega(0)$ is the forward differential elastic cross section. In contrast, the normal correction referred to earlier is just given by the second factor in parentheses above. The first factor in parentheses was, for most of the targets in our experiment, 48.8.

The correction given by Eq. (19) is $< 0.05\%$ in the case of the hydrogen measurement and has been neglected.

In the case of the heavy elements, the approximations used in arriving at Eq. (19) were not valid. We calculated the corrections using Monte Carlo techniques as follows: K_2^0 mesons were generated at the internal target and followed through the attenuation target. Account was taken of absorption, of single and plural scattering, of the target boundaries, and of the finite source size. A "black sphere" interaction, with nuclear radius obtained from the measured total cross section, was assumed²⁵; and a Gaussian approximation to $d\sigma^{el}/d\Omega(\theta)$ was used. In this way the angular distribution at the target exit of particles scattered at least once was obtained. The fraction of such events accepted by the collimator was then computed externally. These calculations were performed for each heavy element at several momenta. Results at the other momenta were obtained by interpolation. The resulting percentage corrections to be applied to the measured total cross sections are given in Table VIII. The measured total cross sections are to be *increased* in making the corrections. The numbers are in qualitative, but not quantitative, agreement with the results of a naive application of Eq. (19). We have applied the corrections.

The total cross sections for ~ 67 -nsec ghost K 's are expected to be larger than the corresponding cross

²⁵ J. M. Blatt and V. F. Weisskopf, *Theoretical Nuclear Physics* (John Wiley & Sons, Inc., New York, 1952), Chap. VIII.

FIG. 10. K_2^0 -nuclear cross sections.

sections for "good" K 's, because the cross sections tend to decrease with momentum (as will be seen). We have estimated the effects of the ghosts in the case of the heavy-element measurements as follows: (1) Assume that the ghost cross section is infinite; (2) calculate the resulting correction to the "good" K total cross section; and (3) divide the result by two. The percentage correction to the beryllium cross sections (the worst case) obtained using this procedure is tabulated versus momentum in column 2 of Table VIII. The corrections are quite small, but we have applied them in the case of the heavy elements.

The ~ 33 -nsec ghosts at a given momentum consist of contribution from K mesons ~ 33 nsec later in true flight time, and also earlier. The contributions may be obtained by shifting the spectrum appropriately and by multiplying by the fraction of internal beam in the wrong bunches, which was 0.002 in the case of the heavy elements. In the momentum range 160–350 MeV/ c the *late* ghosts in the spectrum with no targets were negligible in comparison with "good" K 's because of the shape of the spectrum (cf. Fig. 8). The 0.002 factor is enhanced by the spectrum shape in the case of the *early* ghosts, typically by a factor of 5, over an appreciable part of the spectrum. However, corrections to the total cross sections would be necessary only to the extent that the total cross sections for ghosts and "good" K 's are considerably different. This is not true in our case. Specifically, the correction to the total

cross section is less than $\frac{1}{2}\%$ in every case and is less than $\frac{1}{10}$ of the statistical error in every case. We have therefore neglected the alternate-bunch effects upon the heavy-element measurements.

In the case of the hydrogen measurement, in contrast to the above, the correction for ~ 67 -nsec ghosts is negligible and that for the early ~ 33 -nsec ghosts is appreciable. The carbon in the beam in the case of the hydrogen measurement had the effect of "sharpening" the spectrum (cf. Fig. 8) so that the early ~ 33 -nsec ghost effect was enhanced by a larger factor than in the case of the heavy elements; and the alternate-bunch fraction was larger as well, averaging 0.0044 during the hydrogen measurement. On the other hand, the carbon in the beam attenuated ~ 67 -nsec ghosts more than "good" K 's, so that the ~ 67 -nsec ghost fraction was less than in the case of the heavy-element measurements. The late ~ 33 -nsec ghosts were negligible for the same reasons as in the heavy-element case. The fraction of ~ 67 -nsec ghosts with carbon in the beam may be estimated by extrapolating the carbon spectrum in Fig. 8 (after first subtracting the "plug" background) to later flight times and by shifting the resulting curve ~ 67 nsec earlier. This procedure yields a ghost fraction of typically 3×10^{-4} between 160 and 350 MeV/ c . Accordingly, we have neglected the ~ 67 -nsec ghost effect in the hydrogen measurement. For the early ~ 33 -nsec ghosts, we have evaluated the effects upon the cross-section measurements in a straightforward fashion under the assumption that the ghost cross sections are the measured cross sections with the spectrum shifted appropriately, extrapolating to higher momenta where necessary. The corrections to be applied to the measured hydrogen total cross sections are given in column 3 of Table VIII. The effect is to increase the cross section by typically 1%. We have made the corrections.

Some of the targets contained significant amounts of impurities (see Table II). However, the effect of a given impurity upon the cross-section measurements was significant only to the extent that its ratio of total cross section to atomic number differed from that of the principal element in the target. These ratios were sufficiently insensitive to atomic number so that the effects were small. We have calculated the appropriate corrections from the spectroscopic analysis of the targets, using interpolation (in atomic number) of our total cross-section data to obtain the cross sections for the impurities. No iteration was necessary. The percentage corrections to be applied to the cross sections are given in the 12th row of Table VIII. They are independent of momentum to an adequate approximation. We have made the corrections.

An over-all normalization uncertainty is present for each target. Our estimates of these scale uncertainties are given in the last row of Table VIII. They include the uncertainties in the numbers of particles/area (cf. Table II), and also our estimates in the uncertainties in

the corrections discussed in this and in the preceding section. The scale uncertainties have not been included in the quoted errors for individual measurements.

Our *final* results for the K_2^0 - p and K_2^0 -nuclear total cross sections are given in Table IX.

The hydrogen cross sections will be discussed in Sec. IV. The heavy-element cross sections are plotted versus momentum in Fig. 10 (the iron cross sections are omitted for the sake of clarity; they are similar to the copper cross sections). It is seen that the cross sections decrease with momentum, to an appreciable extent for the lighter elements, and to a lesser extent for the heavier elements. A log-log plot of the total cross sections versus atomic number (A) at the highest momentum, 343 MeV/ c , is shown in Fig. 11. The cross sections at this momentum roughly obey a power-law dependence in A which is neither linear nor $A^{2/3}$, but some intermediate power. The A dependence at lower momenta (not shown in Fig. 11) is less steep than at 343 MeV/ c . If the momentum dependence of the cross sections shown in Fig. 10 were to be extrapolated to momenta higher than those considered here, then the A dependence would approach something closer to linearity than to $A^{2/3}$. This would be surprising. We have not attempted to understand the heavy-element cross sections further (e.g., in terms of nuclear models).

We would like to add a word of caution concerning the interpretation of the statistical errors quoted in Table IX. The errors at a given K momentum are not completely independent. They were determined from the diagonal elements of the variance matrices of the background fit which was discussed in Sec. III C (except that they were scaled according to the corrections discussed in the present section). However, the off-diagonal elements of these matrices are not negligible; they are typically 20% of the diagonal elements. Thus a quantitative fit of the cross sections at given momentum versus atomic number to some power law, for example, would not be statistically correct, strictly speaking, without the inclusion of the off-diagonal terms. To list these terms in the present paper would require eleven additional tables; thus we have not given them.

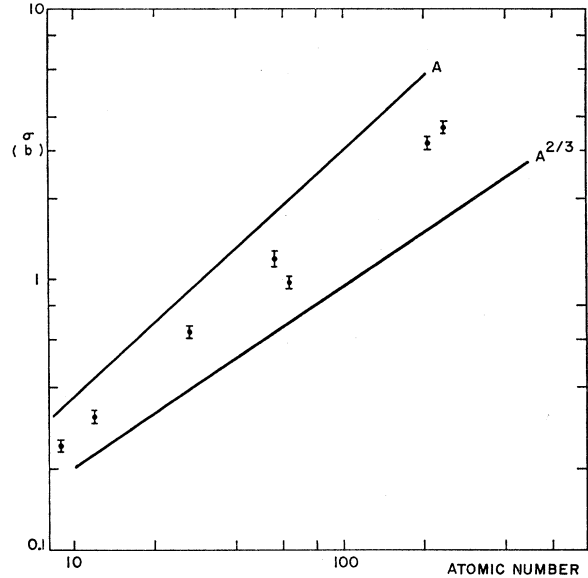


FIG. 11. Log-log plot of the K_2^0 -nuclear cross sections versus atomic number of 343 MeV/ c . Lines with slopes appropriate to an A and to an $A^{2/3}$ dependence, respectively, are shown.

E. Analysis of the Mean Life Measurement

The differential velocity spectrum of our K detector should obey

$$\frac{1}{M_L} \left(\frac{dN_L(v)}{dv} \right) \propto \epsilon(L) \exp \left[-\frac{t(1-v^2/c^2)^{1/2}}{\tau} \right], \quad (20)$$

where v and t are the nominal velocity and flight time [see Eqs. (2) and (3)] for detector position L ; τ is the K_2^0 mean life; N_L and M_L are the numbers of detector and monitor counts, respectively, with the detector at position L ; and $\epsilon(L)$ is the K_2^0 detection efficiency (or, equivalently, the detector "solid angle") at position L . Equation (20) is expressed in terms of quantities directly measured in the experiment, of the desired mean life, and of the efficiency. The absolute efficiency at one particular detector position may be absorbed into the proportionality constant and need not be known;

TABLE IX. Final total cross-section results.^a

Corrected momentum (MeV/ c)	Cross sections in mb				Cross sections in barns			
	H	Be	C	Al	Fe	Cu	Pb	U
343	26.0± 2.9	242±10	308± 7	638±26	1.18±0.08	0.969±0.044	3.14±0.14	3.64±0.15
308	30.4± 3.5	269±11	336± 8	683±29	1.24±0.11	1.146±0.060	3.26±0.17	3.72±0.16
281	31.0± 3.9	265±12	361± 9	703±31	1.41±0.15	1.111±0.062	3.40±0.18	3.82±0.17
358	33.7± 4.6	316±14	391±11	750±35	1.14±0.07	1.23 ±0.10	3.09±0.16	3.61±0.17
239	46.4± 5.5	311±14	411±12	793±38	1.29±0.15	1.25 ±0.09	3.67±0.22	3.95±0.20
223	38.6± 6.2	332±16	429±14	850±46	1.51±0.30	1.21 ±0.11	3.54±0.24	3.84±0.21
209	41.9± 6.1	341±16	430±14	799±41	1.19±0.10	1.19 ±0.08	3.32±0.19	4.13±0.23
197	51.5± 7.8	390±20	456±15	845±51	1.46±0.23	1.39 ±0.13	3.73±0.27	4.19±0.27
187	50.2± 9.2	385±22	477±18	860±55	1.50±0.24	1.37 ±0.12	3.35±0.24	4.35±0.28
177	50.1± 9.7	355±23	445±21	722±52	1.08±0.10	1.17 ±0.11	3.62±0.30	3.97±0.28
168	70.1±15.0	476±37	481±24	963±89	1.54±0.47	1.31 ±0.19	3.55±0.41	4.29±0.39

^a The quoted errors were determined from the variance matrices of the residual background fits, except that they were scaled directly according to the magnitudes of the other corrections to the cross sections. The scale uncertainties for the various elements have not been included.

knowledge of the fractional *change* in efficiency with position is sufficient for determination of the mean life from the data. The proportionality constant at each given velocity may be determined by comparing spectra at different detector positions.

As will be seen, the purely statistical error in our mean life determination was $\sim 2\frac{1}{2}\%$, and it was therefore necessary to understand the detection efficiency variation with position as well as possible. The only effect known to us which caused such a variation was the divergence of the neutral beam. In general, one would expect the resulting changes in the beam profile with distance to cause corresponding changes in the detector efficiency. We calculated the efficiency variation by first making Monte Carlo calculations of the efficiencies for beam profiles corresponding to the various detector positions, and then by taking the ratios. This is described in the following paragraphs.

The basic Monte Carlo program had the following features: Hypothetical K_2^0 mesons of given momentum were allowed to decay along the beam line with vertex positions whose transverse geometric distribution was that of the beam distribution at the detector position in question, including umbra, penumbra, and the asymmetry produced by the attenuation of the proton beam in the internal target. The events were distributed among the various charged decay modes in accordance with known branching ratios.²⁶ The $V-A$ weak-interaction Hamiltonian was used to calculate the center-of-mass energy and angular distributions for the leptonic modes, with the f^+/f^- ratio taken from experiment,²⁶ and the decay distributions were weighted accordingly. Range requirements corresponding to the material in the counter telescopes were imposed. The exact geometry of the counters and of the iron absorbers [including the slight asymmetries shown in Fig. (3)] was included. The absolute efficiencies obtained from this program are those which, after inserting a number for the actual rate of decay into charged modes, were given in Table I. The program was also used to generate the time distributions for light collection which were discussed in Sec. III A.

The organization of the program was such that it could be run for different beam profiles, hence different detector positions, using the *same* set of random numbers. This procedure reduced the "statistical error," i.e., the error caused by running the program for only a finite number of hypothetical events, in the *difference* in efficiencies for two beam profiles to a negligible level. This is true because such a difference is approximately distributed according to the binomial distribution, as can be shown; and if the numbers of hypothetical counts for two different profiles are almost equal, which was true in our case, then the error in the difference in counts is just the square root of the difference.

In operating the program, a fixed number of hypothetical events were generated for the beam profile appropriate to each detector position (26, 31, 36, and 41 ft). The efficiency in each case was obtained by comparing the number of detected events with the number of generated events. The detected events numbered about 10^4 per program run with given beam profile and K momentum and varied by about 1% over the range of detector positions. The statistical error, in the sense discussed above, in the *difference* of the efficiency corresponding to two different given detector positions was thus of order 10^{-3} of the efficiency itself. Series of program runs were taken with the input parameters changed in accordance with the uncertainties in their values. Series were also taken with different sets of random numbers.

Our best estimates for the fractional variation of efficiency with distance ($d\epsilon/\epsilon$) are: -0.043 per 15-ft displacement away from the target with only opposite counter-telescope pairs considered; 0.058 for adjacent pairs; and -0.012 for the complete detector. We estimate the uncertainty in the last number to be ± 0.006 . This uncertainty is essentially the spread in the calculated $d\epsilon/\epsilon$ for various reasonable values of the input parameters and for various sets of random numbers. The efficiency was a linear function of detector position and the fractional efficiency variation was independent of K momentum, to good approximations.

The efficiency variations were also calculated using a different Monte Carlo program. This program included essentially the same features as those described above, but was different in detailed philosophy. The two sets of results for the fractional efficiency variations agreed within their uncertainties.

The fact that the efficiency variation of our detector was small may be seen, qualitatively, from the following considerations: Assume that the beam profile is symmetric (attenuation in the internal target affects only the penumbra). Assume that the detector efficiency for a *single* decay particle as a function of the transverse position of the decay vertex is known. With the coordinate origin at the center of the detector, expand the efficiency in a Taylor series in the ratios of the transverse vertex coordinates to the half-width of the detector. Neglect the small asymmetries in the detector (cf. Fig. 3). Then only even terms occur in the series because of the fourfold symmetry of the detector. Average the efficiency over a beam profile of width X (over one dimension only, for simplicity). The ratio of the average of the quadratic term to that of the constant term is then of order $X^2/3W^2$, where W is the full width of the detector. The quantity $X^2/3W^2$ was about 0.02 for our detector at the 26-ft position, and about 0.05 at the 41-ft position. The *difference* in these numbers, which would give the order of magnitude of the fractional efficiency variation, is about 0.03. However, this would be the effect for a single decay particle. With *two* particles the effect would be further reduced

²⁶ G. H. Trilling, Argonne National Laboratory Report No. ANL-7130, 1965 (unpublished).

TABLE X. Analysis of K_2^0 mean life.

Detector positions	Telescope combinations	Nominal momenta (MeV/c)	Efficiency variation, $d\epsilon/\epsilon$ per 15 ft	Fitted mean life (nsec) ^a	χ^2	Degrees of freedom	χ^2 probability
All	All	180-280	-0.012	51.7±1.3	110.77	109	44%
All	AC	180-280	-0.043	49.0±2.0	118.35	109	25%
All	BD	180-280	-0.043	50.3±2.2	88.77	109	92%
All	Adjacents	180-280	+0.058	53.3±2.3	106.05	109	57%
Omit 26 ft	All	220-300	-0.014	49.4±1.9	66.52	79	54%
Omit 31 ft	All	220-300	-0.014	52.9±1.4	81.39	71	19%
Omit 36 ft	All	220-300	-0.014	52.5±1.5	75.65	71	34%
Omit 41 ft	All	220-300	-0.014	53.9±2.0	76.62	79	54%
All	All	220-300	-0.014	52.5±1.4	104.09	103	46%
All	All	200-240	-0.014	54.3±1.9	59.82	48	12%
All	All	200-270	-0.014	52.1±1.4	99.35	87	17%
All	All	200-300	-0.014	53.4±1.3	130.61	126	37%
All	All	200-330	-0.014	54.2±1.2	163.60	165	52%
All	All	200-360	-0.014	56.0±1.2	237.13	204	5%
All	All	200-390	-0.014	57.6±1.2	300.50	243	1%

^a Errors are statistical only, determined from the variance matrices.

to the extent that the directions are uncorrelated. This is because moving the decay vertex away from the detector center would cause the solid angles of opposite telescopes to change in opposite directions. Therefore, the value of 0.012 for the efficiency variation obtained from the Monte Carlo calculations is not unreasonable.

We next discuss the actual statistical analysis of the data. The individual data runs were tested for stability by summing the spectra over the useful momentum region and by comparing the counting rates for different runs at the same detector position. The stability was good except for two runs, one at 26 ft and the other at 41 ft. The counting rate for each of these runs differed by more than three standard deviations from the average for all runs at the corresponding detector position. These runs were not included in the data analysis and this corresponds to a rejection of about 12% of the available data. The effect of including these runs would have been to raise our final result for the mean life slightly.

The data were grouped into bins of width 10 MeV/c in K momenta. This binning procedure is essentially the integration of Eq. (20) over velocity intervals of variable width. The data in the same momentum (or velocity) bins at different detector positions were compared in implementing Eq. (20). In cases where the end point of a bin was at some fraction of an analyzer channel, the corresponding fraction of the number of counts in that channel was used in the bin. The data in a given bin with given detector position for the various sets of telescope combinations were added together for the purpose of arriving at a final result for the mean life, but were analyzed separately for the purpose of testing internal consistency. The values used for the kinematic quantities were the nominal values obtained from Eqs. (2) to (4).

The "plug-closed" and ~ 67 -nsec ghost backgrounds (see Sec. II E) were subtracted from each bin, at each distance, and for each telescope combination. For this

purpose, the measured ghost spectrum at 31 ft was propagated to the other distances using a value for the K_2^0 mean life which, for the final analysis, was our final result, i.e., an iterative procedure was used. The small statistical errors in the backgrounds were included in calculating the statistical errors in the corrected spectra. The effects of the alternate-bunch background (Sec. II E) and of the residual beam-associated background (Sec. III D) will be discussed later.

The analysis was performed using a least-squares fit to the data. The variable parameters for the fit were the K_2^0 mean life and one dummy parameter for each momentum bin which was proportional to the K flux in that bin at the internal target. These dummy parameters are essentially the proportionality constants appropriate to Eq. (20), but with the inclusion of the absolute detection efficiency. Specifically, the χ^2 function for the fit was

$$\chi^2 = \sum_{i,k} \left\{ \frac{N_{ik}}{M_i} - n_{0k} \left[1 + \left(\frac{d\epsilon}{\epsilon} \right)_i \right] \right. \\ \left. \times \exp \left[-\frac{t_{ik}(1-v_k^2/c^2)^{1/2}}{\tau} \right] \right\}^2 / (\sigma_{ik}/M_i)^2. \quad (21)$$

The i sum is over data runs and the k sum over momentum bins; the N_{ik} and M_i are the numbers of counts in the detector (with background subtracted) and monitor, respectively; σ_{ik} is the statistical error in N_{ik} ; $(d\epsilon/\epsilon)_i$ is the fractional efficiency variation for position i relative to that at 26 ft and was obtained as described earlier (the efficiency variations appropriate to opposite, adjacent, or all telescope combinations were used, depending on which data were being fitted); the n_{0k} are the dummy parameters; and the kinematic quantities are the nominal values, evaluated at the center of the bin. The n_{0k} and τ were varied until (21) was minimized and the statistical errors in these quantities were computed from the variance matrix at the minimum.

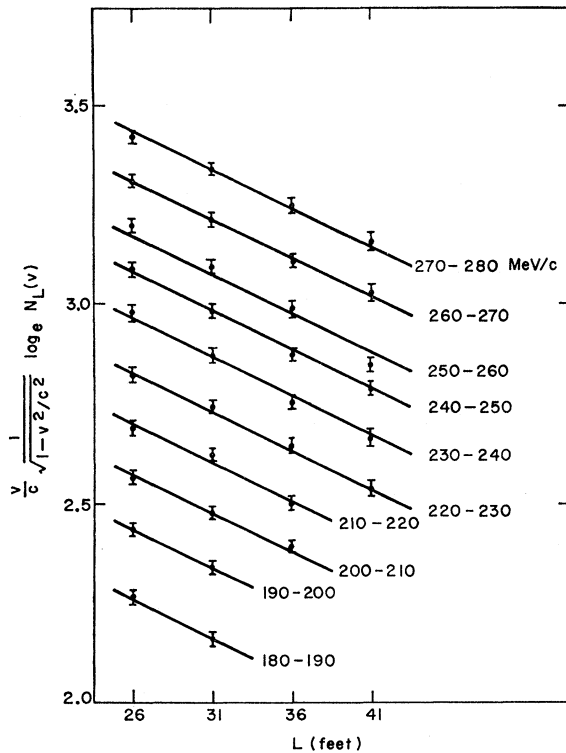


FIG. 12. Plot of all data used in obtaining the final result for the K_2^0 mean life. The ordinate is explained in the text. The lines shown have slopes appropriate to a mean life of 51.7 nsec.

The results of fits using various subsets of the data are tabulated in Table X. The χ^2 obtained from Eq. (21), degrees of freedom, χ^2 probability, the fitted mean life, and its associated statistical error are given. The first line in the table will be discussed shortly. The next several lines show various internal consistency checks. The second, third, and fourth lines pertain to fits using the three independent sets of telescope combinations separately. The three sets of data are independent and are clearly consistent. The χ^2 for their deviations about their weighted mean (not the same χ^2 as that in the table) is 2.0 for 2 degrees of freedom. The next four lines in the table show the effects of omitting data at given detector positions. The lower momentum cutoff for these fits is such that exactly the same momentum bins are included at all detector positions. The fits are not independent, but their consistency may be studied by comparing the mean lives with the result obtained using distances with the same momentum interval. This latter fit is given in the next line. The χ^2 for the deviations about this mean is 3.2 and the correct number of degrees of freedom is 2; this yields a 20% χ^2 probability. Thus there do not appear to be distance-dependent systematic effects outside of statistical errors.

The next several lines in Table X show the effect of varying the upper momentum cutoff. There is a clear trend for the fitted mean life to increase as more momentum bins are included. The fits also become rather poor,

as may be seen from the χ^2 probabilities given in the table, when the highest momenta are included. The effect is essentially that which was shown in Fig. 9. It may be associated with the residual beam-associated background which was discussed in Sec. III C in connection with the total cross-section measurements, as that background was such that its ratio to the K_2^0 counting rate increased with momentum. The fitted mean lives nevertheless appear stable for cutoffs of 300 MeV/c and below.

The fit which gives our final result (prior to small corrections) for the mean life is shown in the first line in Table X. The lower momentum cutoff was chosen to be 180 MeV/c for the data with the detector at 26 and at 31 ft, 200 MeV/c at 36 ft, and 220 MeV/c at 41 ft. This excludes at least the ten latest channels of the pulse-height analyzer in all cases; it also excludes the flight-time region wherein there was a second peak in the "plug-closed" spectrum at 26 ft (see Fig. 8). The upper momentum cutoff is 280 MeV/c for all detector positions and was chosen for two reasons: (1) The fitted mean lives are stable within statistical errors for cutoffs near this value in the case of fits using all telescope combinations, as was just mentioned, and also for fits using individual combinations. (2) If one calculates the detector threshold for an $(n,2p)$ reaction in the wall of the vacuum pipe (see Fig. 3), assuming a neutron with the same flight time from the internal target as that of the K_2^0 with respect to which the process would represent a background, then the corresponding K momentum is 320 MeV/c.

Our result for the K_2^0 mean life prior to final corrections is then $\tau = (5.17 \pm 0.13) \times 10^{-8}$ sec. The statistical error is thus $\pm 2\frac{1}{2}\%$.

The data used in the final fit are shown in Fig. 12 in the form of a plot of $(v/c)(1 - v^2/c^2)^{-1/2} \log_e N_L(v)$ versus L . For each point, the $N_L(v)$ is the sum of all the data at detector position L in the appropriate momentum interval, and the quantity $(v/c)(1 - v^2/c^2)^{-1/2} = \hbar c/mc^2$ is averaged over the momentum interval. The data should fall on straight lines with slope $(-1/c\tau)$. The straight lines shown in the figure correspond to a value of 51.7 nsec for the mean life τ .

We next discuss some systematic effects which were not included in the above statistical analysis. First, there is the question of the residual background which was fitted in the total cross-section analysis of Sec. III C. Averaging the results given in Table VI for this background over telescope combinations and over the momentum range used in the mean life analysis yields the result that the background with no targets in the beam was about $1\frac{1}{2}\%$ of the K rate. The dependence of this fraction upon detector position is unknown as total cross sections were measured at 26 ft only. We consider the following hypotheses for the distance dependence: (1) Assume the background-to- K ratio to vary linearly from 1.5% at 26 ft to zero at 41 ft. Then we estimate that our result for the mean life is too small by 2.4% of

its value. That is, if we were to correct the result for this assumed background, then the correction would *raise* our result. (2) Assume the absolute background rate to vary according to the solid angle subtended by the K detector at the internal target. Then our result is too small by 0.6% of its value. (3) Assume the absolute background to vary according to the solid angle subtended by the detector at the collimator exit. Then our result is too small by 1.8%. (4) Assume that the background was produced at the collimator exit, but not isotropically, and further assume (for the sake of definiteness) that its angular distribution was the same as that of the electron pairs used for time calibrations (see Sec. II D). Then our result is too small by 0.6%. (5) Finally, assume the distance dependence to be the same as that of the measured "plug-closed" background (see Sec. II E). Then our result for the mean life is too *large* by 0.6%.

The most reasonable hypothesis for the distance dependence of the residual background seems to us to be a falling off with distance from the collimator exit, but with the solid-angle factor partially compensated by the forward peaking characteristic of the diffraction scattering of high-energy neutrons. The effect upon the mean life measurement would then be similar to case (4) above. If this were true, then the error caused by not correcting for the presence of this background would be about $\frac{1}{4}$ of the statistical error. Large effects caused by the residual background seem to be precluded because the mean lives determined using different telescope combinations agree within their errors (see lines 2, 3, and 4 in Table X; and recall that the effects of the background upon the counting rates in the various combinations were different, as discussed in Sec. III C). For these reasons, we have not attempted to correct our result for the mean life to account for the presence of this background. Neither have we modified our estimate of the uncertainty in the mean life.

The fraction of the internal beam in the "wrong" alternate phase-stable bunches averaged to 0.0018 during the mean life measurement. For the momentum range used in the mean life analysis, the resulting "late" ~ 33 -nsec ghosts were negligible in comparison with the "early" ghosts, for the same reasons as in the total cross-section analysis (see Sec. III D). We have calculated the resulting effect upon the mean life determination by generating fictitious spectra including ~ 33 -nsec early ghosts, by comparing rates to obtain quasi-measured mean lives, by comparing the results with the mean life used to generate the spectra, and by taking an appropriate average over momenta and over pairs of detector positions. The result is that in order to correct for the presence of this alternate-bunch effect, our result for the mean life is to be decreased by 0.5% of its value. We have made this correction. The uncertainty in the correction is 0.1% of the mean life itself and thus may be neglected.

TABLE XI. Measurements of the K_2^0 mean life.

Measurement	Mean life (nsec)
Bardon <i>et al.</i> ^a	81_{-24}^{+32}
Darmon <i>et al.</i> ^b	51_{-13}^{+24}
Astbury <i>et al.</i> ^c	61_{-12}^{+15}
Fujii <i>et al.</i> ^d	53 ± 5
This experiment	51.5 ± 1.4

^a M. Bardon, K. Lande, L. M. Lederman, and W. Chinowsky, *Ann. Phys. (N. Y.)* **5**, 156 (1958).

^b J. Darmon, A. Rousset, and J. Six, *Phys. Letters* **3**, 57 (1962).

^c P. Astbury, A. Michelini, C. Verkerk, F. Verkerk, W. Beusch, M. Pepin, and M. A. Pouchon, *Phys. Letters* **18**, 178 (1965).

^d T. Fujii, J. Jovanovich, F. Turkot, G. T. Zorn, and M. Deutsch, in *Proceedings of the Twelfth International Conference on High-Energy Physics, Dubna, 1964* (Atomizdat, Moscow, 1966).

The effects of corrections to the nominal flight times, of timing uncertainties, and of time resolution (including effects caused by binning the data and by taking fractions of analyzer channels) were considered in Sec. III A. These effects are negligible.

Our Monte Carlo calculation of the distance dependence of the detection efficiency (or "detector solid angle") was uncertain to some degree. The efficiency changed by $1.2\% \pm 0.6\%$ of its value in moving the detector through the full range of positions, as discussed earlier in this section. We estimate this 0.6% uncertainty in the distance dependence to produce a corresponding uncertainty in the mean life of 1.0% of its value. We have included this latter uncertainty in our estimate of the uncertainty in the final result.

Our final result for the K_2^0 mean life is

$$\tau = (5.15 \pm 0.14) \times 10^{-8} \text{ sec.} \quad (22)$$

This is compared with previous determinations of the mean life in Table XI.

IV. \bar{K}^0 - p s -WAVE SCATTERING LENGTH

We have fit our K_2^0 - p total cross-section data to the Dalitz-Tuan parameterization of the low-energy $\bar{K}N$ system in terms of s -wave scattering lengths.⁴ This is described in this section.

We assume that K -nucleon scattering at sufficiently low energies is due to s waves alone. We also assume that the s -wave phase shift in each channel with definite isotopic spin and strangeness is determined by a single complex parameter, the scattering length for that channel:

$$\cot \delta = 1/kA, \quad (23)$$

where δ is the phase shift, k is the center-of-mass wave number, and A is the scattering length. Equation (23) is expected to be valid at sufficiently low energy, and this is equivalent to saying that the "effective-range term" is negligible. The total cross section for the single channel case is then

$$\sigma = 4\pi \frac{a^2 + b^2 + b/k}{k^2 a^2 + (1 + kb)^2}, \quad (24)$$

TABLE XII. Results of scattering length fit.

Momentum interval (MeV/c)	$ \bar{a}_1 ^a$ (F)	\bar{b}_1^a (F)	Degrees of freedom $P(\chi^2)$		
			χ^2	of freedom	$P(\chi^2)$
168-187	0.00 ± 0.21	0.64 ± 0.11	0.9	1	35%
168-209	0.00 ± 0.14	0.64 ± 0.07	1.3	3	73%
168-223	0.00 ± 0.14	0.62 ± 0.06	1.5	4	82%
168-239	0.18 ± 0.13	0.65 ± 0.06	3.6	5	61%
168-281	0.03 ± 0.12	0.65 ± 0.05	3.8	7	92%

^a Errors are statistical only, determined from the variance matrices.

where a and b are the real and imaginary parts, respectively, of the scattering length A .

The K_2^0 - p total cross section at given momentum is the average of the corresponding K^0 - p and \bar{K}^0 - p total cross sections [cf. Eq. (9)]. The K^0 - p system is an equal mixture of the isotopic spin states $T=0$ and $T=1$, while the \bar{K}^0 - p system is a pure $T=1$ state. We define the scattering lengths A_0 and A_1 for K^0 - p , and \bar{A}_1 for \bar{K}^0 - p , in accordance with Eq. (23). The quantities A_0 and A_1 are real because there is no absorption in the KN system at low energies. From Eqs. (9) and (24), the K_2^0 - p total cross section may then be written as

$$\sigma_2 = 2\pi \left[\frac{1}{2} \frac{a_1^2}{1+k^2 a_1^2} + \frac{1}{2} \frac{a_0^2}{1+k^2 a_0^2} + \frac{\bar{a}_1^2 + \bar{b}_1^2 + \bar{b}_1/k}{k^2 \bar{a}_1^2 + (1+k\bar{b}_1)^2} \right], \quad (25)$$

where $a_1 = A_1$, $a_0 = A_0$, and $\bar{a}_1 + i\bar{b}_1 = \bar{A}_1$.

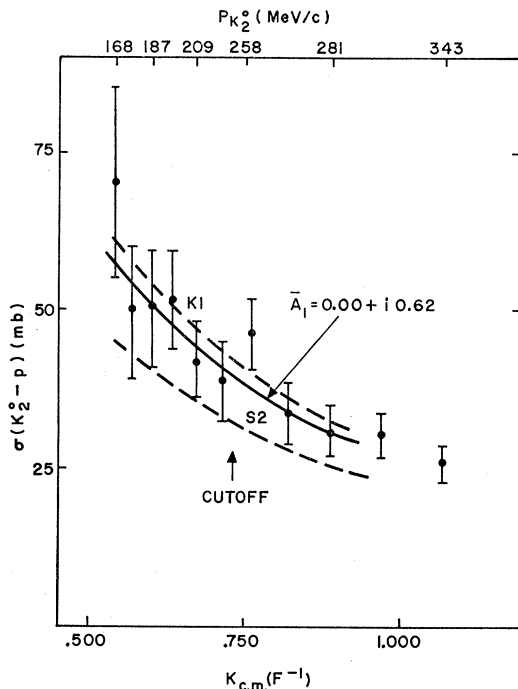


FIG. 13. K_2^0 - p total cross-section results. The three curves correspond to \bar{K}^0 - p total cross sections predicted by the parameters given in Table XIII, averaged with K^0 - p total cross sections predicted by $a_1 = -0.30$ F, $a_0 = 0.04$ F.

We have fitted the hydrogen total cross sections which are given in Table IX to Eq. (25).

The magnitudes of the various quantities in Eq. (25) are such that the first two terms are small in comparison with the third. Accordingly, we have assumed the present best values (known to us) of -0.30 F²⁷ and 0.04 F²⁸ for a_1 and a_0 , respectively, and have allowed \bar{a}_1 and \bar{b}_1 to vary in fitting the data. The uncertainties in a_1 and a_0 are ± 0.01 F²⁷ and ± 0.04 F²⁸, respectively; these uncertainties have a negligible effect upon the uncertainties in our final results for \bar{a}_1 and \bar{b}_1 .

The results of fits for various momentum intervals are given in Table XII. The lower cutoff was 168 MeV/c and the upper cutoff variable. We have chosen an upper cutoff of 223 MeV/c for the final result. The results are obviously stable above and below this cutoff. This shows that neither a nonzero effective range nor p -wave scattering affect the determination of \bar{A}_1 appreciably (their effects upon the total cross section would to lowest order be proportional to k^2 and k^3 , respectively). The χ^2 for the fit with the 223-MeV/c cutoff is 1.5 for 4 degrees of freedom; this yields a χ^2 probability of 82%, indicating an excellent fit. Thus our result for the $\bar{K}N$ isotopic spin-1 s -wave scattering length is

$$\bar{A}_1 = (0.00 \pm 0.14) \text{ F} + i(0.62 \pm 0.06) \text{ F}. \quad (26)$$

The off-diagonal terms in the variance matrix are negligible; therefore the errors in \bar{a}_1 and \bar{b}_1 may be considered to be independent.

There have been several previous determinations of \bar{A}_1 .⁴⁻⁷ They were all derived from K^- - p partial cross-section measurements using hydrogen bubble chambers. A brief summary of the differences between this method and ours is in order. First there is the question of the measurements themselves. The normalization of the cross sections in the case of the bubble-chamber method depends upon the understanding of scanning efficiencies, whereas our normalization depends most critically upon understanding of the background (cf. Sec. III C). Determination of the incident momentum is somewhat difficult in the bubble-chamber case because the K^- mesons typically are slowing down rapidly due to ionization loss near the interaction points; in our case the incident momentum is known to typically $\pm 4\%$ from the time of flight. Then there is the question of determining \bar{A}_1 from the measurements. In the bubble-chamber case much more information is available than in our experiment; many different partial cross sections may be measured in the former case while we only measure total cross sections. On the other hand, our study of the K_2^0 - p system effectively isolates the isotopic spin-1 part of the $\bar{K}N$ interaction while the K^- - p determinations of \bar{A}_1 are complicated by the

²⁷ S. Goldhaber, W. Chinowsky, G. Goldhaber, W. Lee, T. O'Halloran, T. F. Stubbs, G. M. Pjerrou, D. H. Stork, and H. K. Ticho, Phys. Rev. Letters **9**, 135 (1962).

²⁸ V. J. Stenger, W. E. Slater, D. H. Stork, and H. K. Ticho, Phys. Rev. **134**, B1111 (1964).

presence of the isotopic spin-0 part, which is considerably larger, and also by the Coulomb amplitude. The K^-p determinations have tended to yield two possible sets of parameters which fit the data. (This ambiguity may be associated, at least roughly, with the division of the interaction into isotopic spin states; as it has been resolved to some level of significance with the inclusion of charge-exchange measurements,^{7,8} and conclusively by recent measurements of K_2^0-p partial cross sections.²⁹) Our χ^2 function, on the other hand, has a single minimum.

Our value of \bar{A}_1 is compared with the two most recent and most statistically significant of the bubble-chamber K^-p determinations in Table XIII. Total K_2^0-p cross sections predicted by the three values (again assuming -0.30 and 0.04 F for a_1 and a_0 , respectively) are shown in Fig. 13, along with our data. The data and also our determination of \bar{A}_1 are in excellent agreement with the determination by Kim.⁷ A fit of the data between 168 and 223 MeV/ c to the central value of his result yields a χ^2 probability of 89% . The same comparison with the result of Sakitt *et al.*⁶ yields a probability of 18% , perhaps indicating marginal disagreement. A stronger statement could be made if higher momenta were included in the comparison, as is evident by inspection of Fig. 13; however, we do not feel that our understanding of the possibilities of a nonzero effective range and of p waves is sufficient to make such a comparison. In view of the discussion in the preceding paragraph, the agreement that does exist between our results and the bubble-chamber results strikes us as being significant.

In principle, other variable parameters in addition to \bar{A}_1 could be included in fitting our total cross-section data and one could obtain information on (1) the KN s -wave scattering lengths a_0 and a_1 ; (2) effective ranges; and (3) p waves. In practice, the data are only sensitive to \bar{A}_1 and we can shed no light upon these other questions.

V. CONCLUSIONS

We have developed a K_2^0 detection system which can usefully detect of order 5000 events per hour with

²⁹ J. A. Kadyk, Y. Oren, G. Goldhaber, S. Goldhaber, and G. H. Trilling, Phys. Rev. Letters 17, 599 (1966).

TABLE XIII. Determinations of \bar{A}_1 .

Determination	\bar{a}_1 (F)	\bar{b}_1 (F)
Kim ^a (K_1)	-0.07 ± 0.06	0.68 ± 0.03
Sakitt <i>et al.</i> ^b (S_2)	-0.19 ± 0.08	0.44 ± 0.04
This experiment	$\pm 0.00 \pm 0.14$	0.62 ± 0.06

^a Reference 7.

^b Reference 6; we have given only the solution which has not been conclusively excluded by Kadyk *et al.*, Ref. 29.

typical momentum resolution of $\pm 4\%$. We have demonstrated that the peculiar time structure of the Princeton-Pennsylvania accelerator may be relied upon as the sole means of kinematic identification of secondary neutral particles. The injector chopping system facility has been shown to function adequately.

We have measured the K_2^0 mean life to be $(5.15 \pm 0.14) \times 10^{-8}$ sec; and we have measured K_2^0-p total cross sections to typically $\pm 15\%$ per bin of width equal to the resolution width, and K_2^0 -nuclear cross sections to considerably better accuracies. The isotopic-spin-1 $\bar{K}N$ s -wave scattering length has been determined from the K_2^0-p data to be $(0.00 \pm 0.14) F + i(0.62 \pm 0.06) F$, in fair agreement with previous determinations.

In addition to the principal results of the experiment listed above, we have measured the K_2^0 production spectrum at 93° from 2.8 -GeV protons incident upon 1.5 -in. platinum (see Sec. II C), we have put a constraint upon the integrated γ flux under the same conditions (Sec. II B), and we have verified by direct measurement that the relativistic velocity limit is the speed of light, to about $\frac{1}{2}\%$ (Sec. III A).

ACKNOWLEDGMENTS

We are especially grateful to H. Allen, Dr. C. L. Kang, and other members of the Accelerator Operations Division who built and operated the hardware for the chopping system. We thank Dr. P. Boynton and C. Martin for assistance with the measurements. One of us (E.B.) would like to thank the members of the General Relativity Group at the University of Maryland for their hospitality during portions of this work. The support of Professor M. G. White and the staff of the Princeton-Pennsylvania accelerator is gratefully acknowledged.